

## Novel nanoSchiff base M(II) and M(III) complexes derived from antiviral valacyclovir and 2-hydroxy-1-naphthaldehyde (HNAPB). Structural characterization, bio-efficiency, DNA interaction, molecular modeling, docking and conductivity studies

Khadija M.Nassir<sup>1</sup>, MosadA. El-ghamry \*<sup>2</sup>, Fatma M.Elzawawi<sup>1</sup>, Ayman A. Abdel Aziz<sup>1</sup>, Samy M. Abu-El-Wafa<sup>2</sup>

<sup>1</sup>(Department of Chemistry, Faculty of Science, Ain Shams University, Abbasia, Cairo, Egypt)

<sup>2</sup>(Department of Chemistry, Faculty of Education, Ain Shams University, Roxy, Cairo, Egypt)

**Abstract:** A novel Schiff base ligand, H<sub>2</sub>L, 2-[(2-[(2-hydroxy-naphthalen-1-ylmethylene)amino]-6-oxo-1H-purine-9-yl)methoxy]ethyl-2-amino-3-methylbutanoate derived from antiviral valacyclovir has been prepared (HNAPB). The nano-sized Cr(III), Mn(II), Co(II), Ni(II), Cu(II) and Zn(II) of the ligand, HNAPB (H<sub>2</sub>L), were synthesized by different methods. The nano-sized crystalline phases for the complexes particles were indicated by XRD patterns and supported by TEM images. Characterization of the ligand and its complexes were performed using elemental analysis, IR, UV-Vis, <sup>1</sup>HNMR, ESR, Mass, TGA, conductivity and magnetic susceptibility measurements. The associated water and/or EtOH molecules with the complexes were confirmed by TGA data. The geometrical structures of complexes under investigation were confirmed by the results of UV-Vis, ESR spectra, magnetic moment measurement and molecular studies. The bond lengths of the ligand were different than those of the complexes, especially for azomethine N-atom, C(2)-N(23), C(24)-N(23) = 1.399, 1.323 Å, and naphtholate O-atom, C(30)-O(31) = 1.350 Å, which coordinated with the metal ions. The calculated azomethine (C=N) and naphtholate (C-O) bond lengths in all metal complexes were found to be in the range 1.320 - 1.500 and 1.296 - 1.395 Å, respectively, indicating slightly elongation of these bonds due to coordination with the metal ions. The antitumor activity of the ligand, H<sub>2</sub>L, and its nano-sized metal complexes was investigated against Hepatocellular carcinoma cell line (HepG-2 cells). The nano-sized Cu(II) complexes V, XXIV and XXVI exhibited strong antitumor activities. The nano-sized Cu(II) complex XXIV (which synthesized in media SO/EtOH) exhibited IC<sub>50</sub> value (1.93 µg/ml) smaller than the standard drug cis-platin (3.27 µg/ml), indicating the high efficiency of this nano-sized complex as antitumor agent towards HepG-2 cells. The DNA cleavage study showed the ability of nano-sized Cu(II) complex V to degrade DNA, and the nano-sized Cu(II) complex XXIV surrounding to DNA and carried out necrosis. The docking results revealing strong interactions of both the ligand, H<sub>2</sub>L, and its Cu(II) complex V with DNA. The antibacterial and antifungal activities of the ligand, H<sub>2</sub>L, and its nano-sized metal complexes were screened against different types of organisms. The results showed marked enhancement in activity on coordination with the metal ions. The electrical properties of nano-sized Cu(II) complexes V, XXIII and XXVI were investigated. The temperature dependence of A.C. conductivity ( $\sigma_{ac}$ ) was described and the activation energies ( $E_a$ ) were calculated for the complexes by using the Arrhenius plot. The obtained results revealed that these complexes had semiconducting properties. The calculated values of charge carrier concentration and mobility indicated that the conduction process occurs by a hopping mechanism.

**Key words:** nano-sized metal complexes, green synthesis, spectral, antitumor, DNA interaction, docking, conductivity

Date of Submission: 02-05-2020

Date of Acceptance: 16-05-2020

### I. Introduction

Antiviral drugs are important in cure or control virus infections [1]. Valacyclovir is an orally active prodrug of the antiviral drug acyclovir [2], and exhibits antiviral activity against herpes simplex virus (HSV) types 1 (HSV-1) and 2 (HSV-2) and varicella zoster virus (VZV) in vitro and in vivo [3-6]. Recently, complexation has often been used to influence biological processes that are metal dependent [7, 8]. The application of diagnostic metal complexes to medicine is a rapidly developing therapeutic field [9]. The Schiff bases complexes have a broad wide range in coordination chemistry and nano coordination particles have received much attention because of their distinctive optical, magnetic, electrical, and catalytic properties, also due to their biological activities [10-12]. The green synthesis of nano coordination particles, using the natural ingredients

present in plant extracts, offers an alternative, efficient, inexpensive, and environmentally friendly method to produce well-defined geometries of nanoparticles [13].

No literature have been found the studied nano-sized metal complexes so the purpose of the present work was to prepare a novel Schiff base, 2-[(2-[(2-hydroxy-naphthalen-1-ylmethylene)amino]-6-oxo-1H-purine-9-yl)methoxy]ethyl-2-amino-3-methyl butanoate ligand, HNAPB ( $H_2L$ ), derived from the reaction between antiviral drug valacyclovir with 2-hydroxy-1-naphthaldehyde, Scheme 1, and its nano-sized metal(II) and metal(III) complexes with some of the transition metals. The nano-sized metal complexes were prepared by chemical synthesis using EtOH or CTAB/EtOH mixture, and green synthesis using *Spinaciaoleracea* (SO) or *Malvaparviflora* (MP) extract in EtOH. The ligand and its complexes were characterized by elemental and thermal analyses, IR, UV-Vis,  $^1H$ NMR, ESR and Mass spectra, XRD and TEM, as well as conductivity and magnetic susceptibility measurements. In addition, antimicrobial and antitumor activities, DNA interaction, molecular modeling and docking have been studied.

## II.Experimental

### 2.1. Materials

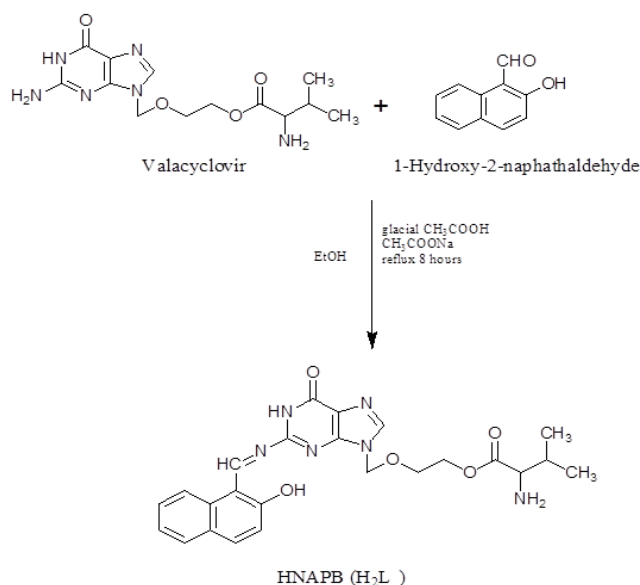
Metal salts:  $CuCl_2 \cdot 2H_2O$ ,  $NiCl_2 \cdot 6H_2O$ ,  $ZnCl_2$ ,  $CoCl_2 \cdot 6H_2O$ ,  $MnCl_2 \cdot 4H_2O$  and  $CrCl_3 \cdot 6H_2O$ , Valacyclovir, 2-hydroxy-1-naphthaldehyde, CTAB, EDTA,  $LiOH \cdot H_2O$ , nitric acid were Aldrich. BDH or Merck products. The solvents used were ethanol, methanol, DMF and diethylether. These solvents were purified by the recommended methods [14].

### 2.2. Instruments and working procedures

The apparatus and working procedures on these studies are the same as previously described elsewhere[15-17].

### 2.3. Synthesis of the Schiff base Ligand HNAPB ( $H_2L$ )

A mixture of valacyclovir (1.62 gm, 5 mmol) and 2- hydroxynaphthaldehyde (0.86 gm, 5 mmol) in absolute ethanol (50 ml) with 1ml of glacial acetic acid and 0.3 gm sodium acetate anhydrous was refluxed for 8 hours. The product was allowed to cool till room temperature, filtered off and recrystallized from ethanol then dried under vaccum to give yellow crystals, yield 83 %, m.p.  $160^\circ C$ . The proposed formula of the ligand ( $C_{24}H_{26}N_6O_5$ , F.W. = 478) is in good agreement with the stoichiometry concluded from analytical data and mass spectra, scheme 1:



**Scheme 1:** Synthesis of the ligand,  $H_2L$ .

### 2.4. Synthesis of the Metal Complexes

Ethanol solutions of the ligand,  $H_2L$ , and the metal salt,  $CuCl_2 \cdot 2H_2O$ ,  $NiCl_2 \cdot 6H_2O$ ,  $CoCl_2 \cdot 6H_2O$ ,  $MnCl_2 \cdot 4H_2O$ ,  $ZnCl_2$  or  $CrCl_3 \cdot 6H_2O$  were mixed in a 1:1 (L:M) molar ratio. The resulting solutions were refluxed on a hot plate from 6 to 8 hours according to the same procedures observed in our publications [15, 16]. The solid complexes which separated on hot were filtered off, washed with hot ethanol, bidistilled water and diethylether and finally dried in vacuum desiccator over anhydrous  $CaCl_2$ . All of the complexes prepared, **I**, **II**,

**III, IV, V and VI**, were stable at room temperature, non-hygroscopic, insoluble in common organic solvents except DMF. The analytical and physical data for the metal complexes are collected in Table 1.

## 2.5. Synthesis of Nano-sized Complexes

### 2.5.1. Preparation of Plant Leaves Extracts

The fresh green leaves (20 g) of *Spinaciaoleracea* (SO) plant or *Malvaparviflora* (MP) plant were washed with double-distilled water and dried at room temperature. The dry plant was crushed and extracted by adding 100 ml of a mixture of ethanol/water (70%) and standing for one week at room temperature. The extract was filtered off; the filtrate was collected, and used in the green synthesis of nano-sized metal complexes.

### 2.5.2. Chemical and Green Synthesis of Nano-sized Complexes

Nano-sized metal complexes of the Schiff base ligand,  $H_2L$ , have been prepared by chemical synthesis using CTAB/EtOH mixture [18], and green synthesis using *Spinaciaoleracea* (SO) or *Malvaparviflora* (MP) extract in EtOH [19], by adding 4 ml of 0.01 M of Schiff base ligand,  $H_2L$ , in ethanol dropwise to dry beaker contains 40 ml of CTAB ( $3 \times 10^{-2}$  M), SO extract (20%) or MP extract (20%) in ethanol and 4 ml of 0.01M of metal salt,  $CuCl_2 \cdot 2H_2O$ ,  $NiCl_2 \cdot 6H_2O$ ,  $CoCl_2 \cdot 6H_2O$ ,  $MnCl_2 \cdot 4H_2O$ ,  $ZnCl_2$  or  $CrCl_3 \cdot 6H_2O$  in ethanol. The reaction mixture was stirred on a magnetic stir plate for about 4 hours, then leave from 2-7 days. The obtained solid nano-sized metal complexes (CTAB/EtOH, SO/EtOH, MP/EtOH): Cr(III) complexes (**VII, VIII, IX**), Mn(II) complexes (**XI, XII, XIII**), Co(II) complexes (**XV, XVI, XVII**), Ni(II) complexes (**XIX, XX, XXI**), Cu(II) complexes (**XXIII, XXIV, XXV**) and Zn(II) complexes (**XXIX, XXX, XXXI**) were filtered off, washed with ethanol and finally dried in vacuum desiccator over anhydrous  $CaCl_2$ .

## III. Results and Discussion

### 3.1. Characterization of the Ligand, $H_2L$

The structure of the Schiff base Ligand HNAPB ( $H_2L$ ) was investigated by elemental analyses, IR,  $^1H$ NMR, UV-Vis, and mass spectra. Anal. Calcd. %: C, 60.25; H, 5.44; N, 17.57. Found %: C, 60.84; H, 5.93; N, 17.94. The IR spectrum ( $cm^{-1}$ ) of the ligand, Table 2, showed characteristic bands at 3471, 3176, 1725, 1686, 1624, 1608, 1307 and 1098, corresponding to  $\nu(OH)$ naphtholic,  $\nu(NH)$ ,  $\nu(C=O)$ ester,  $\nu(C=O)$ amide,  $\delta(NH)$ ,  $\nu(C=N)$ azomethine,  $\nu(C-N)$ , and  $\nu(C-O)$ , respectively [20]. The electronic absorption spectrum,  $\lambda_{max}(nm)$ , of the ligand ( $10^{-3}$  M in DMF), showed three characteristic bands at 297, 350 and 400 which can be assigned to  $\pi-\pi^*$  transition within the aromatic system,  $\pi-\pi^*$  transition within  $C=N$  and an intramolecular charge transfer (CT) transition within the whole molecule. The mass spectrum of HNAPB, Figure 1, showed the molecular ion peak at  $m/e = 478$  amu, confirming its formula weight (F.W. = 478). The mass fragmentation pattern, shown in Scheme 2, supported the suggested structure of the HNAPB.

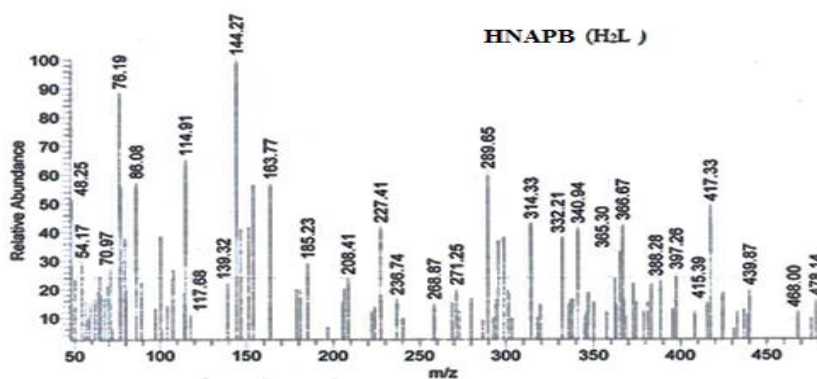
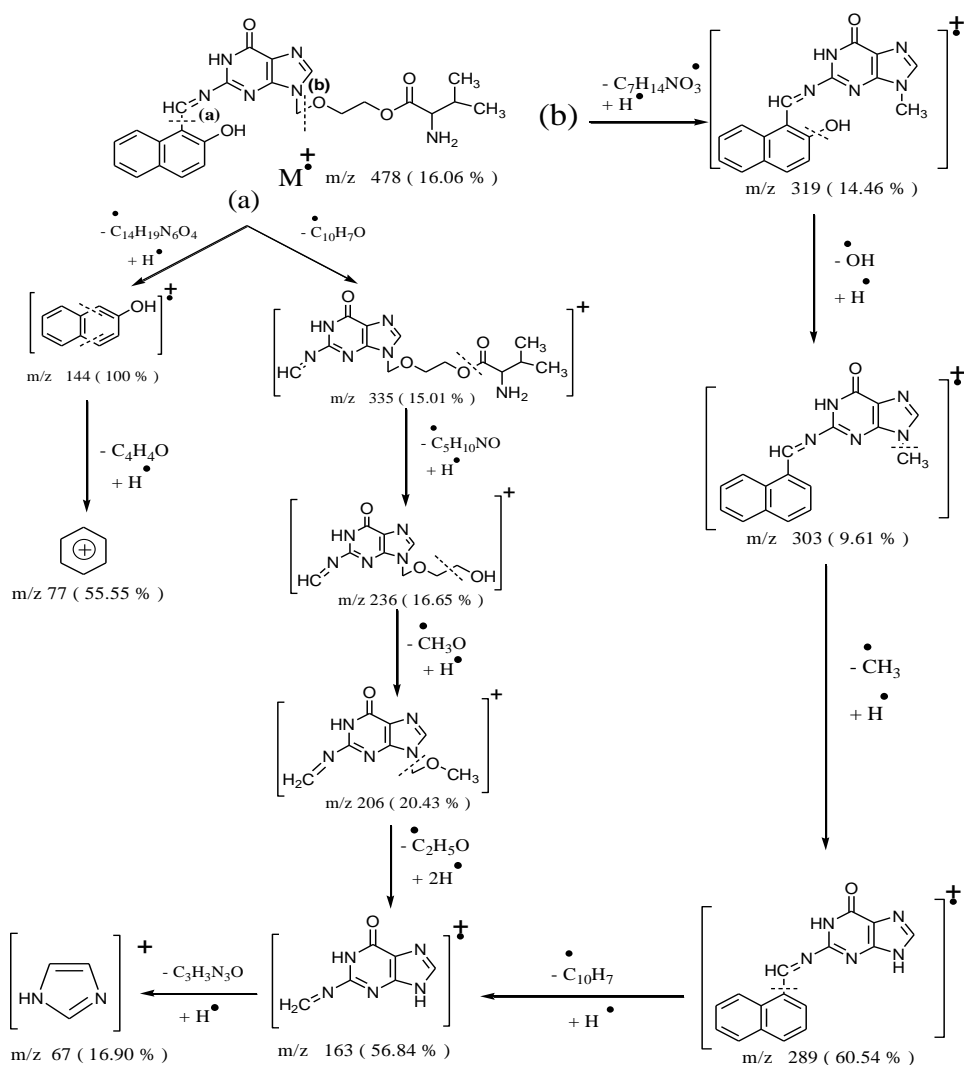


**Figure 1:** Mass spectrum of the ligand,  $H_2L$ .



Scheme 2: Mass fragmentation pattern of the ligand, H<sub>2</sub>L.

### 3.2. Characterization of the Metal Complexes

According to elemental analysis, the metal complexes of the ligand, H<sub>2</sub>L, were assigned to possess the compositions and molecular formulae listed in Table 1. The results indicated that the ligand, H<sub>2</sub>L, acts as bidentate towards the metal ions in a mono-deprotonated form via the azomethine – N and the phenolic – O atoms, in a molar ratio 1 : 1 (M : L) for complexes III; V; VI, and 1 : 2 (M : L) for complexes I; II; IV.

Molar conductivities ( $\Omega_m$ ) of the metal complexes were measured in DMF ( $10^{-3}$  M) and collected in Table 1. The complexes I, II, III, IV, V and VI have  $\Omega_m$  values in the range 5.73 – 39.70  $\text{ohm}^{-1} \text{cm}^2 \text{mol}^{-1}$  which indicated the non-electrolytic nature of all complexes [21]. The observed  $\Omega_m$  values of some complexes may be due to the displacement of part of coordinated Cl<sup>-</sup> ions by DMF solvent molecules [22].

**Table 1:** Analytical and physical data of metal complexes of the ligand HNABP (H<sub>2</sub>L).

No.	Complex	Molecular Formula	Colour	m.p. (°C)	%Yield	M.Wt (gm/mol)	Elemental analysis, found % (calcd %)				Ω <sub>m</sub> (ohm <sup>-1</sup> cm <sup>2</sup> mol <sup>-1</sup> )
							% C	% H	% N	% M	
I	[Cr(HNABP) <sub>2</sub> (H <sub>2</sub> O)Cl].3H <sub>2</sub> O	C <sub>48</sub> H <sub>58</sub> N <sub>12</sub> O <sub>14</sub> ClCr	green	>300	73	1113.4	52.04 (51.73)	5.51 (5.21)	15.64 (15.09)	5.57 (4.66)	5.73
II	[Mn(HNABP) <sub>2</sub> (H <sub>2</sub> O) <sub>2</sub> ].2H <sub>2</sub> O	C <sub>48</sub> H <sub>58</sub> N <sub>12</sub> O <sub>14</sub> Mn	brown	>300	55	1080.9	53.15 (53.29)	5.84 (5.37)	16.02 (15.54)	6.49 (5.07)	11.31
III	[Co(HNABP)(EtOH)Cl].H <sub>2</sub> O	C <sub>26</sub> H <sub>33</sub> N <sub>6</sub> O <sub>8</sub> ClCo	brown	>300	76	635.4	49.01 (49.10)	5.24 (5.19)	13.63 (13.22)	9.46 (9.27)	11.73
IV	[Ni(HNABP) <sub>2</sub> (H <sub>2</sub> O) <sub>2</sub> ].3H <sub>2</sub> O	C <sub>48</sub> H <sub>60</sub> N <sub>12</sub> O <sub>15</sub> Ni	brown	>300	58	1102.6	52.30 (52.24)	5.29 (5.44)	14.51 (15.24)	5.01 (5.31)	39.7
V	[Cu(HNABP)(H <sub>2</sub> O)Cl]	C <sub>24</sub> H <sub>27</sub> N <sub>6</sub> O <sub>8</sub> ClCu	green	>300	64	594.0	48.50 (48.48)	4.69 (4.55)	14.14 (14.14)	10.54 (10.69)	27.9
VI	[Zn(HNABP)(H <sub>2</sub> O)Cl].2.5H <sub>2</sub> O	C <sub>24</sub> H <sub>32</sub> N <sub>6</sub> O <sub>8.5</sub> ClZn	yellow	>300	60	640.8	44.91 (44.94)	5.47 (5.00)	13.10 (13.10)	9.93 (10.19)	9.75

### 3.2.1. Infrared Spectra

The IR spectrum of the ligand, H<sub>2</sub>L, was compared to those of the metal complexes, in order to ascertain the coordination sites that might be involved in the chelation. The characteristic bands, of the free ligand and its metal complexes, and their assignments are listed in Table 2. All complexes **I**, **II**, **III**, **IV**, **V** and **VI** showed a broad band in the range 3416 –3468 cm<sup>-1</sup> assigned to ν(OH) of the H<sub>2</sub>O and/or EtOH molecules associated with the complexes, which were confirmed by elemental and thermal analyses. The IR spectrum of the ligand displayed characteristic band at 3471 cm<sup>-1</sup> which is assigned to ν(OH)naphtholic frequency. The absence of this band in the IR spectra of all solid complexes is clear evidence that the coordination process proceed with the deprotonation of the naphtholic OH group [23]. The band due to ν(C=N), which observed at 1608 cm<sup>-1</sup> in the IR spectrum of the free ligand, shifted appreciably to lower wave number by 27 – 33 cm<sup>-1</sup> in the IR spectra of all solid complexes, suggesting the involvement of nitrogen atom of the azomethine group in the bonding with the metal ion [24]. The characteristic vibrations of the (C=O)amide of the purinone moiety, as well as (C=O)ester of the aliphatic side chain were almost unaffected by the complexation thereby, excluding the possibility of their bonding to the metal ions. The nature of metal – ligand bonding is confirmed by the newly formed bands at 505 – 571 and 477 –433 cm<sup>-1</sup> in the spectra of the complexes which are tentatively assigned to ν(M–O) and ν(M–N), respectively [25, 26].

**Table 2:** Important IR spectral data and their assignment for the ligand HNABP (H<sub>2</sub>L) and its metal complexes.

No.	Compound or Complex	IR Spectral bands (cm <sup>-1</sup> )										
		ν(OH) H <sub>2</sub> O EtOH	ν(OH) naphtholic	ν(NH)	ν(CH) aromatic	ν(CH) aliphatic	ν(C=O) ester	ν(C=O) amide	δ(NH)	ν(C=N) azomethine	ν(M-O)	ν(M-N)
	HNABP (H <sub>2</sub> L)	---	3471	3176	3048	2962	1725	1686	1624	1608	---	---
I	[Cr(HNABP) <sub>2</sub> (H <sub>2</sub> O)Cl].3H <sub>2</sub> O	3468	---	3175	3039	2964	1727	1683	1625	1575	531	477
II	[Mn(HNABP) <sub>2</sub> (H <sub>2</sub> O) <sub>2</sub> ].2H <sub>2</sub> O	3465	---	3183	3034	2965	1728	1682	1627	1575	558	433
III	[Co(HNABP)(EtOH)Cl].H <sub>2</sub> O	3465	---	3176	3036	2963	1729	1682	1628	1575	505	438
IV	[Ni(HNABP) <sub>2</sub> (H <sub>2</sub> O) <sub>2</sub> ].3H <sub>2</sub> O	3462	---	3168	3034	2964	1729	1686	1627	1576	566	471
V	[Cu(HNABP)(H <sub>2</sub> O)Cl]	3458	---	3115	3033	2963	1730	1684	1620	1581	571	458
VI	[Zn(HNABP)(H <sub>2</sub> O)Cl].2.5H <sub>2</sub> O	3416	---	3202	3034	2964	1726	1680	1628	1575	506	443

### 3.2.2. <sup>1</sup>HNMR Spectra

<sup>1</sup>HNMR spectrum, Figure 2, gives further support of the suggested structure of the ligand, H<sub>2</sub>L. <sup>1</sup>HNMR spectral data (δ ppm) of the ligand relative to TMS in DMSO-d<sub>6</sub> without and with D<sub>2</sub>O showed signals at 0.87-0.90 [d, 6H, 2CH<sub>3</sub>], 2.2 [m, 1H, -CH(CH<sub>3</sub>)<sub>2</sub>], 3.72 [t, 2H, -OCH<sub>2</sub>], 4.23 [d, 1H, -CH-NH<sub>2</sub>], 4.36 [t, 2H, CH<sub>2</sub>OCO], 5.37 [s, 2H, NCH<sub>2</sub>O], 6.67 [s, 2H, -NH<sub>2</sub>], 6.82-7.84 [m, 6H, Ar-H], 8.13 [s, 1H, Ar-H 5-membered ring], 9.2 [s, 1H, CH=N], 10.8 [s, 1H, NH (disappeared on adding D<sub>2</sub>O)], 14.64 [s, 1H, OH (completely disappeared on adding D<sub>2</sub>O)] [27]. The <sup>1</sup>HNMR spectrum of Zn(II) complex (**VI**), Figure 2, was measured to confirm the mode of bonding between the ligand, H<sub>2</sub>L, and the metal ion. The singlet observed at δ 14.64 ppm due to the phenolic – OH proton present in the free ligand is absent in the Zn(II) complex indicating deprotonation of the phenolic – OH group through coordination with the metal ion. The value (δ 9.2 ppm) of azomethine proton(-CH=N-), in the free ligand, was shifted to lower field (δ 9.33 ppm) indicating chelation of azomethine-N atom with the metal ion. These results support and agree with the data obtained from IR spectral studies.

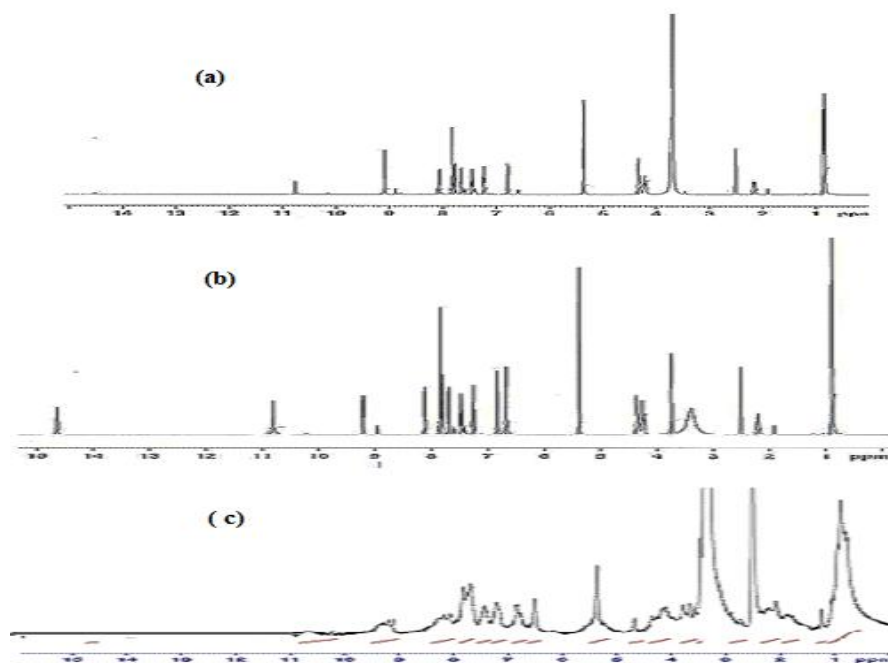


**Figure 2:**  $^1\text{H}$ NMR spectra of the ligand,  $\text{H}_2\text{L}$  (a) with  $\text{D}_2\text{O}$ , (b) without  $\text{D}_2\text{O}$  and its (c)  $\text{Zn}(\text{II})$  complex VI.

### 3.2.3. Thermogravimetric Analysis (TGA)

TGA is used to proof the associated water or solvent molecules to be in the coordination sphere of the complexes or in the crystalline form and supports the elemental analysis, from TG curves, the mass loss was calculated and compared with those theoretically calculated for the suggested formulae based on the elemental analysis [28]. The results of TGA of complexes **I**, **II**, **III**, **IV**, **V** and **VI** were recorded in Table 3. The TG thermograms of these complexes were shown in Figures 3 - 5. These results were found in good agreement with the suggested formulae of the metal complexes listed in Table 1. The complexes **II** and **III** decompose in five steps in the temperature ranges 30.7 – 63.3, 39.8 – 96.8; 64.3 – 203.2, 97.8 – 232.5; 204.2 – 358.7, 233.5 – 367.6; 359.7 – 547.9, 724.6 – 368.6 and 548.9 – 900, 725.6 – 929.6°C. The first step shows elimination of hydrated water. The second weight loss shows removal of coordinated water (for complex **II**) or EtOH molecule (for complex **III**). The third step involves removal of a fragment organic part (for complex **II**) or coordinated  $\text{Cl}^-$  (in a form of HCl) in addition of a fragment organic part (for complex **III**). In the last two steps, the complexes **II** and **III** undergo complete decomposition of the organic part leading to formation of metal oxides, MnO and CoO, as final residues. The TG thermograms of complexes **I**, **IV** and **V** involves four decomposition steps in the temperature ranges 32.1 –

68.8, 30.5 – 74.8, 22.4 – 231.6; 69.8 – 372.0, 75.8 – 121.0, 232.6 – 339.4; 373.0 – 575.3, 122.0 – 470.4, 340.4 – 580.8 and 576.3 – 900.5, 471.4 – 901.50, 581.8 – 902.0 °C. The first step shows removal of hydrated water (for complexes **I** and **IV**) or coordinated water in addition of coordinated  $\text{Cl}^-$  in a form of HCl (for complex **V**). The second step shows elimination of coordinated water and coordinated  $\text{Cl}^-$  in a form of HCl in addition of a fragment organic part (for complex **I**), coordinated water (for complex **IV**) or a fragment organic part (for complex **V**). In the last two steps, the complexes **I**, **IV** and **V** undergo complete decomposition of the remaining organic part leading to formation of  $\text{Cr}(\text{C}_{19}\text{H}_{18}\text{N}_{10}\text{O}_4)$ ,  $\text{Ni}(\text{C}_{11}\text{H}_{18}\text{N}_2\text{O}_2)$ ,  $\text{Cu}(\text{C}_4\text{H}_5\text{NO})$ , respectively, as final residues. The final complex (**VI**) decomposes in only three steps in the temperature ranges 28.2 – 211.9, 212.9 – 347.4, 348.4 – 902.5°C corresponding to loss of hydrated and coordinated water molecules, removal of coordinated  $\text{Cl}^-$  (in a form of HCl) in addition of a fragment organic part and complete decomposition of the remaining organic part leading to formation of ZnO as final residue. The results of TGA showed that decomposition of the metal complexes starts above 200 °C, so these complexes are thermally stable.

**Table 3:** Results of thermogravimetric analysis (TGA) of metal complexes of the ligand HNABP (H<sub>2</sub>L).

Complex No.	Molecular Formula of complex (M.wt)	Temperature range (°C)	Wt loss % Found % (calcd %)	Decomposed product lost
I	[Cr(HNABP) <sub>2</sub> (H <sub>2</sub> O)Cl].3H <sub>2</sub> O (1113.4)	68.8– 32.1	4.77 (4.85)	3 lattice H <sub>2</sub> O
		69.8 – 372.0	21.74 (22.58)	coordinated H <sub>2</sub> O + HCl + C <sub>10</sub> H <sub>17</sub> N <sub>2</sub> O <sub>2</sub>
		373.0 – 575.3	15.31 (15.26)	C <sub>8</sub> H <sub>10</sub> O <sub>4</sub>
		576.3 – 900.5	12.33 (12.21) 45.84 ( 45.07)	C <sub>11</sub> H <sub>4</sub> Residue, Cr(C <sub>19</sub> H <sub>18</sub> N <sub>10</sub> O <sub>4</sub> )
II	[Mn(HNABP) <sub>2</sub> (H <sub>2</sub> O) <sub>2</sub> ].2H <sub>2</sub> O (1080.9)	30.7 – 63.3	3.54 (3.33)	2 lattice H <sub>2</sub> O
		64.3 –203.2	3.36 (3.33)	2 coordinated H <sub>2</sub> O
		204.2 – 358.7	47.58 (47.62)	C <sub>29</sub> H <sub>32</sub> N <sub>2</sub> O <sub>6</sub>
		359.7– 547.9 548.9 – 900.0	24.22 (23.49) 17.14 (16.65) 7.69 (6.55)	C <sub>9</sub> H <sub>2</sub> N <sub>8</sub> O <sub>2</sub> C <sub>10</sub> H <sub>16</sub> N <sub>2</sub> O Residue, MnO
III	[Co(HNABP)(EtOH)Cl].H <sub>2</sub> O (635.4)	39.8–96.8	2.13 (2.83)	lattice H <sub>2</sub> O
		97.8 –232.5	7.56 (7.24)	coordinated EtOH
		233.5 – 367.6	31.02 (30.61)	HCl + C <sub>7</sub> H <sub>12</sub> NO <sub>3</sub>
		724.6 –368.6 725.6 –929.6	27.91 (26.75) 20.50 (20.77) 10.87 (11.78)	C <sub>8</sub> H <sub>2</sub> N <sub>4</sub> O C <sub>9</sub> H <sub>10</sub> N Residue, CoO
IV	[Ni(HNABP) <sub>2</sub> (H <sub>2</sub> O) <sub>2</sub> ].3H <sub>2</sub> O (1102.6)	30.5– 74.8	4.88 (4.89)	3 lattice H <sub>2</sub> O
		75.8 – 121.0	3.28 (3.26)	2 coordinated H <sub>2</sub> O
		122.0 – 470.4	45.69 (45.71)	C <sub>29</sub> H <sub>32</sub> N <sub>2</sub> O <sub>6</sub>
		471.4– 901.5	21.99 (21.77) 24.17 (24.36)	C <sub>8</sub> N <sub>8</sub> O <sub>2</sub> Residue, Ni(C <sub>11</sub> H <sub>18</sub> N <sub>2</sub> O <sub>2</sub> )
V	[Cu(HNABP)(H <sub>2</sub> O)Cl] (594)	22.4 – 231.6	9.89 (9.17)	coordinated H <sub>2</sub> O + HCl
		232.6 – 339.4	24.36 (24.07)	C <sub>7</sub> H <sub>13</sub> NO <sub>2</sub>
		340.4 – 580.8	22.43 ( 21.88)	C <sub>9</sub> H <sub>6</sub> O
		581.8 – 902.0	19.59 (20.20) 23.69 (24.66)	C <sub>4</sub> N <sub>4</sub> O Residue, Cu(C <sub>4</sub> H <sub>5</sub> NO)
VI	[Zn(HNABP)(H <sub>2</sub> O)Cl].2.5H <sub>2</sub> O (640.8)	28.2 – 211.9	9.93 (9.83)	2.5 lattice H <sub>2</sub> O + coordinated H <sub>2</sub> O
		212.9 – 347.4	31.01 (30.35)	HCl + C <sub>7</sub> H <sub>12</sub> NO <sub>3</sub>
		348.4 – 902.5	47.12 (47.08) 11.80 (12.68)	C <sub>17</sub> H <sub>12</sub> N <sub>5</sub> O Residue, ZnO

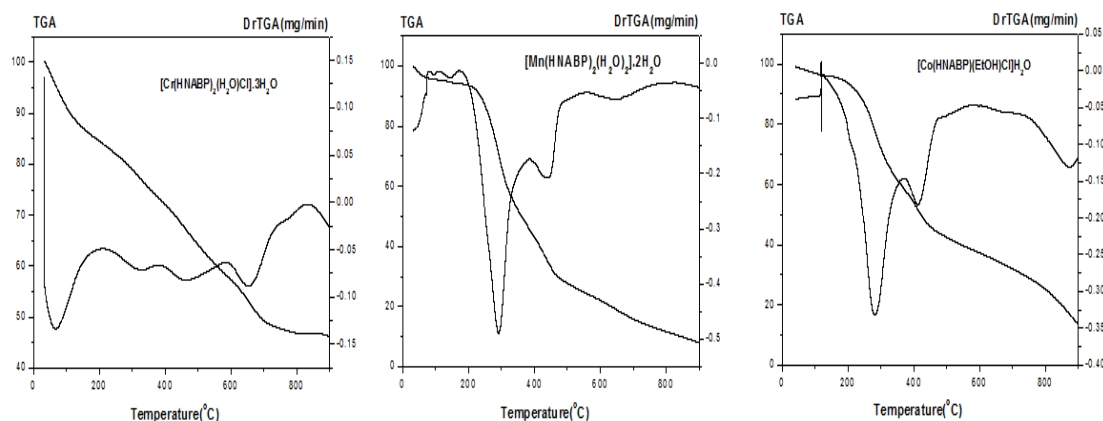


**Figure 3:** TGA – Dr TGA curves of the complexes I, II, and III.

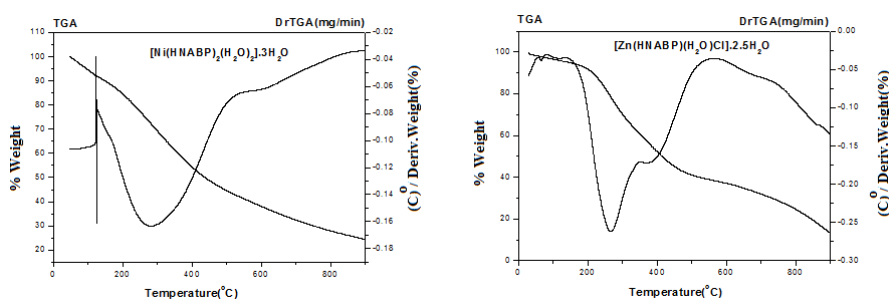


**Figure 4:** TGA – Dr TGA curves of the complexes IV and VI.

TG curves, Figure 5, showed that the nano-sized Cu(II) complexes **V** (in EtOH), **XXIII** (in CTAB/EtOH) and **XXVI** (in CTAB/EtOH, after heating at 200 °C) decompose in three or four stages. The decomposition of these complexes starts at 230, 200 and 250 °C, respectively, indicating the thermal stability of them in the following order: Complex **XXVI** > Complex **V** > Complex **XXIII**. The results, suggesting that the synthesized complexes are thermally stable and in nano-range, so they have large surface area and could be possessed catalytic activity [29].

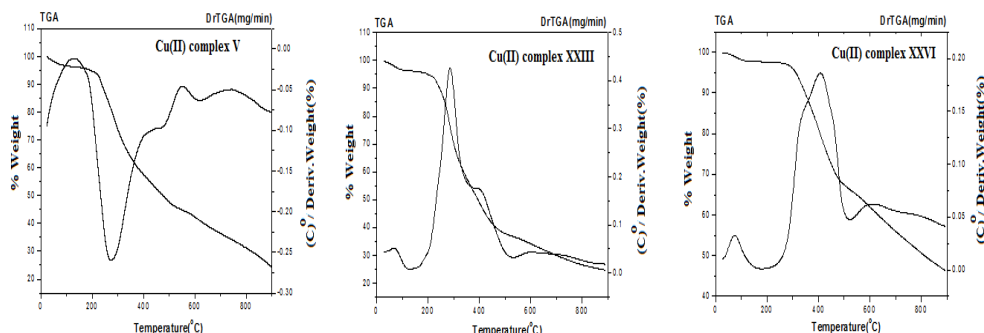


Figure 5: TGA – Dr TGA curves of the Cu(II) complexes V, XXIII and XXVI.

### 3.2.4. Electronic Spectra and Magnetic Measurements

The electronic absorption spectra were measured in DMF ( $10^{-3}$  M), and the magnetic moments (B.M.) were determined at room temperature and support the geometrical structures of the metal complexes. The data obtained are reported in Table 4. The Cr(III) complex (**I**) yielded magnetic moment of 4.31 B.M. which indicates presence of three unpaired electrons in d- orbitals, and close to that expected for an octahedral Cr(III) complexes [30]. This subnormal magnetic moment value (which is around 3.87 B. M.) indicates that the Cr(II) centers are ferromagnetically coupled. The electronic spectrum showed one absorption band at 662 nm, corresponding to the  ${}^4A_{2g}(F) \rightarrow {}^4T_{2g}(F)$  transition, suggesting an octahedral geometry around Cr(III) ion. The electronic spectrum of Mn(II) complex (**II**) showed one absorption band at 588 nm, corresponding to the  ${}^6A_{1g} \rightarrow {}^4T_{2g}(G)$  transition within octahedral structure. The magnetic moment value was 5.05 B. M., which indicating the presence of five unpaired electrons in d- orbitals, and indicating octahedral geometry around Mn(II) ion [31]. The lower value than the expected magnetic moment (which is around 5.92 B. M.) perhaps due to spin – spin antiferromagnetic coupling [32]. The magnetic moment of Co(II) complex (**III**) was found to be 4.88 B.M. This value is consistent with presence of three unpaired electrons in d- orbitals, and confirming tetrahedral geometry around Co(II) ion. The higher value than the expected magnetic moment (which is around 3.87 B. M.) indicated the existence of spin – spin coupling due to ferromagnetic interactions. The electronic spectrum exhibited one absorption band at 675 nm, corresponding to the  ${}^4A_{2g} \rightarrow {}^4T_{1g}(P)$  transition in a tetrahedral configuration [33]. The Ni(II) complex (**IV**) yielded magnetic moment of 3.09 B.M. which indicates presence of two unpaired electrons in d- orbitals, and close to that expected for an octahedral Ni(II) complexes. The electronic spectrum showed two absorption bands at 679 and 746 nm, which can be assigned  ${}^3A_{2g} \rightarrow {}^3T_{1g}(P)$  and  ${}^3A_{2g} \rightarrow {}^3T_{1g}(F)$  transitions within octahedral structure [34]. The electronic spectrum of Cu(II) complex (**V**) showed one absorption band lies at 644 nm, corresponding to the  ${}^2B_{1g} \rightarrow {}^2E_g$  transition, which is in accord with the observed band that characteristic for Cu(II) complex with square planar geometry. In addition, the magnetic moment was 1.74 B.M. which indicates presence of one unpaired electron in d- orbitals, also supporting the square planar geometry for this complex [35].

Table 4: Electronic absorption spectral data (in DMF solution) and magnetic moment values of metal complexes of the ligand HNABP ( $H_2L$ ).

No.	Complex	Colour	Bands assignment due to d-d transition						Magnetic moment values (B. M.)
			$\lambda_{max}$ (nm)	d-d transition	$\epsilon_{max}$ ( $mol^{-1}cm^{-1}L$ )	$\lambda_{max}$ (nm)	d-d transition	$\epsilon_{max}$ ( $mol^{-1}cm^{-1}L$ )	
I	$[Cr(HNABP)_2(H_2O)Cl].3H_2O$	green	662	${}^4A_{2g}(F) \rightarrow {}^4T_{2g}(F)$	45.97	---	---	---	4.31
II	$[Mn(HNABP)_2(H_2O)_2].2H_2O$	brown	588	${}^6A_{1g} \rightarrow {}^4T_{2g}(G)$	37.9	---	---	---	5.05
III	$[Co(HNABP)(EtOH)Cl].H_2O$	brown	675	${}^4A_{2g} \rightarrow {}^4T_{1g}(P)$	24.23	---	---	---	4.88
IV	$[Ni(HNABP)_2(H_2O)_2].3H_2O$	brown	679	${}^3A_{2g} \rightarrow {}^3T_{1g}(P)$	111.4	746	${}^3A_{2g} \rightarrow {}^3T_{1g}(F)$	253.3	3.09
V	$[Cu(HNABP)(H_2O)Cl]$	green	644	${}^2B_{1g} \rightarrow {}^2E_g$	143.7	---	---	---	1.74

### 3.2.5. ESR Spectra

The ESR spectra of Mn(II) complex (**II**), Co(II) complex (**III**) and Cu(II) complex (**V**) were recorded in the solid state at room temperature, as shown in Figure 6, to throw more light about their geometries and the bonding character between the ligand and the metal ion. The X-band ESR spectrum of Cu(II) complex (**V**) exhibited an anisotropic signal with two different g-values,  $g_{||} = 2.07$  and  $g_{\perp} = 2.01$ ,  $g_{av} = 1/3(g_{||} + 2g_{\perp}) = 2.03$ . The g-values together with the profile of ESR signal indicate the square planar geometry around Cu(II) ion. The g tensor values of Cu(II) complex can be used to drive the ground state. The ordering of g values,  $g_{||} (2.07) > g_{\perp} (2.01) > 2.0023$ , indicates the unpaired electron lies predominantly in the  $dx^2-y^2$  orbital giving  $^2B_{1g}$  as the ground state [36]. The  $g_{||}$  value is taken to confirm covalent character of M-L bonds,  $g_{||}$  less than 2.0023 for ionic character and more than 2.0023 for covalent character.  $g_{||}$  (2.07) for Cu(II) complex (**V**) is more than 2.0023, indicating covalent bonding for Cu-L bond [37]. In addition, the g values are taken to calculate the exchange interaction,  $G = (g_{||} - 2)/(g_{\perp} - 2)$ . If  $G > 4$ , the exchange coupling is negligible, whereas when it is less than 4, a considerable exchange interaction is observed in the solid state [38]. The calculated G-value of the Cu(II) complex (**V**) is 7, suggesting absence of exchange coupling between Cu(II) centers in the solid state. The ESR spectrum of Mn(II) complex (**II**) showed a single isotropic line split to six hyperfine lines due to interaction with nuclear spin ( $\frac{5}{2}$ ) of  $^{55}\text{Mn}$  [39]. The  $g_{\text{eff}}$ -value (2.0263) of Mn(II) complex has a positive contribution over that of a free electron (2.0023), indicating covalent nature of bonding between the ligand and the Mn(II) ion. The ESR spectrum of Co(II) complex (**III**) gave one signal split to eight lines due to hyperfine coupling with nuclear spin ( $\frac{7}{2}$ ) of  $^{59}\text{Co}$ . The  $g_{\text{eff}}$ -value of Co(II) complex is 2.0096, which near the free electron value (2.0023).

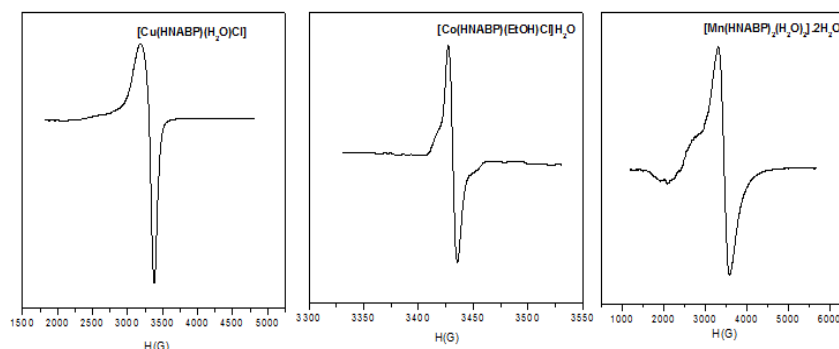


Figure 6: X-band ESR spectra of Cu(II), Co(II) and Mn(II) complexes.

### 3.2.6. Mass Spectra

The mass spectra was performed for Co(II) complex (**III**) Figure 7, as representative example, to confirm this stoichiometry and purity of the complex. The molecular ion peak at  $m/e$  635.58, is coincident with the formula weight of Co(II) complex (Table 1), and the appearance of  $^{58.44}\text{Co}$  and  $^{59.63}\text{Co}$  isotopes with relative intensity 17.25 % and 16.32 %, respectively, support the identity of Co(II) complex structure.

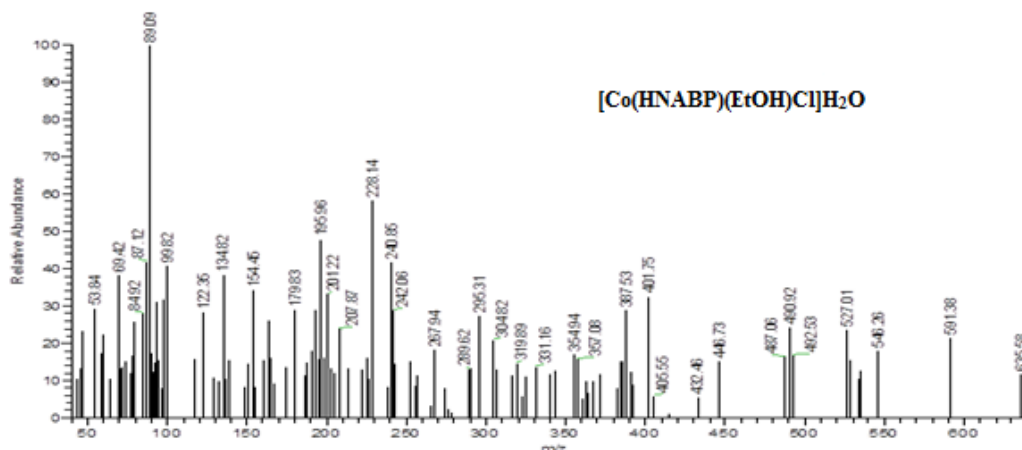


Figure 7: Mass spectrum of the complex III.

### 3.2.7. X-ray Powder Diffraction Studies

X-ray powder diffraction (XRD) analysis is primarily used for phase identification of a crystalline material and can provide information on unit cell dimensions [40]. The diffraction patterns were recorded within diffraction angle ( $2\theta$ ) from  $3^\circ$  to  $80^\circ$ . The X-ray diffractograms of Cr(III) complexes (**I**, **VII**, **VIII**, **IX**), Figure 8, Mn(II) complexes (**II**, **XI**), Co(II) complexes (**XVI**, **XVII**) and Ni(II) complexes (**IV**, **XIX**, **XX**) revealed a series of sharp and intense diffraction peaks which indicate their crystalline characteristic, while for Mn(II) complexes (**XII**, **XIII**), Co(II) complexes (**III**, **XV**), Ni(II) complex (**XXI**) and Cu(II) complexes (**V**, **XXIII**, **XXIV**, **XXV**), the diffraction patterns appear as amorphous. The values of diffraction angles, lattice spacings (d-spacings) and X-ray intensities of different diffraction peaks were measured, and the particle size (crystallite size) of metal complexes were calculated. The particle size can be calculated from X-ray line broadening with help of following Debye Scherrer formula,  $D = K\lambda/\beta\cos\theta$  [41]. Where,  $D$  is the particle size,  $K$  is a coefficient with a value close to unity (it has a typical value is equal to 0.89),  $\lambda$  is the wavelength of X-ray,  $\theta$  is the diffraction angle obtained from  $2\theta$  values corresponding to maximum intensity peak in XRD pattern and  $\beta$  is full width at half maximum. The average particle size, of the complexes **I**, **II**, **IV** (in EtOH), **VII**, **XI**, **XIX** (in CTAB/EtOH), **VIII**, **XVI**, **XX** (in SO/EtOH) and **IX**, **XVII** (in MP/EtOH), Figure 9, was found to be 28.25, 19.82, 22.30, 19.33, 3.00, 21.30, 12.50, 35.16, 31.10, 11.97 and 3.00 nm, respectively, indicating that the complexes particles in nano-sized crystalline phases, and taking the following order: Complex **XI** < Complex **XVII** < Complex **IX** < Complex **VIII** < Complex **VII** < Complex **II** < Complex **XIX** < Complex **IV** < Complex **I** < Complex **XX** < Complex **XVI**.

### 3. 2. 8. Transmission Electron Microscopy (TEM) Studies

The TEM images of nano-sized complexes **I**, **II**, **III**, **IV**, **V** (in EtOH), **VIII**, **XII**, **XVI**, **XX**, **XXIV** (in SO/EtOH), **XXIII** (in CTAB/EtOH) and **XXV** (in MP/EtOH) were performed and TEM micrograph of Cu(II) complexes (**V**, **XXIII**, **XXIV**, **XXV**) were illustrated in Figure 10. The TEM images of the complexes showed spherical shaped particles. The uniformity and similarity in between the particles forms of synthesized complexes indicate that existence of morphological phases have a homogeneous matrix [42]. The average particle size, Figure 11, was found to be 8.25, 9.71, 13.35, 8.05, 10.07, 58.13, 16.80, 9.75, 7.84, 7.03, 12.16 and 1.96 nm for complexes **I**, **II**, **III**, **IV**, **V**, **VIII**, **XII**, **XVI**, **XX**, **XXIII**, **XXIV** and **XXV** respectively, supporting that the complexes in nano-range, and taking the following order: Complex **XXV** < Complex **XXIII** < Complex **XX** < Complex **IV** < Complex **I** < Complex **II** < Complex **XVI** < Complex **V** < Complex **XXIV** < Complex **III** < Complex **XII** < Complex **VIII**. The nano-sized metal complexes in SO/EtOH were heating at  $200^\circ\text{C}$ , and subjected to TEM analysis after heating for 1 hour. The results, Figure 11, showed decrease in particle size from 58.13, 16.80, 9.75, 7.84 and 12.16 for the complexes **VIII**, **XII**, **XVI**, **XX** and **XXIV** to 14.10, 6.15, 1.61, 5.95 and 8.89 for their resulting residues, **X**, **XIV**, **XVIII**, **XXII** and **XXVII**, respectively. While The TEM images, Figure 12, of nano-sized Cu(II) complexes in CTAB/EtOH and MP/EtOH, after heating at  $200^\circ\text{C}$  for 1 hour, showed increase in particle size from 7.03 and 1.96 nm for complexes **XXIII** and **XXV** to 8.05 and 3.55 nm for their resulting residues **XXVI** and **XXVIII**, respectively. Nanoparticle size complexes may possess a variety of biological applications. This is clearly observed in the results of our biological studies of the synthesized nano-sized metal complexes.

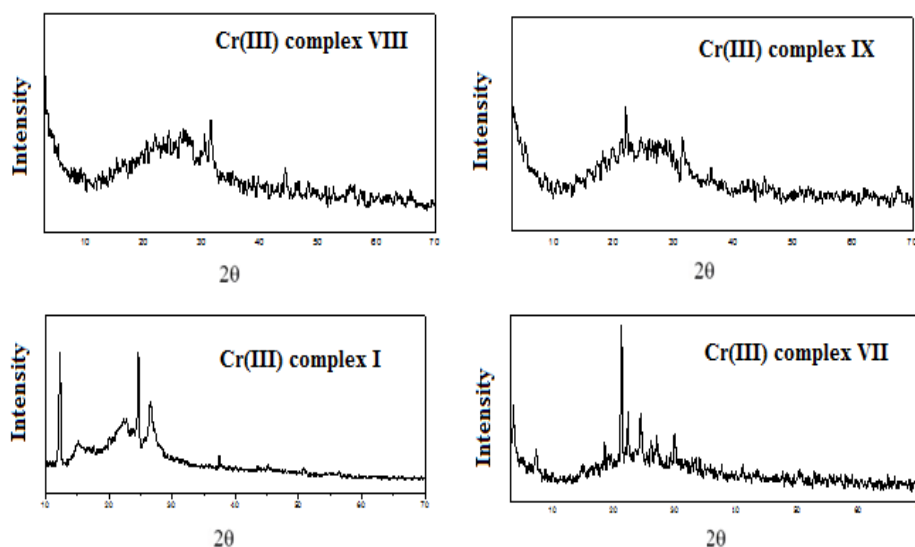


**Figure 8:** X-ray diffraction patterns of the nano-sized Cr(III) complexes I, VII, VIII and IX.

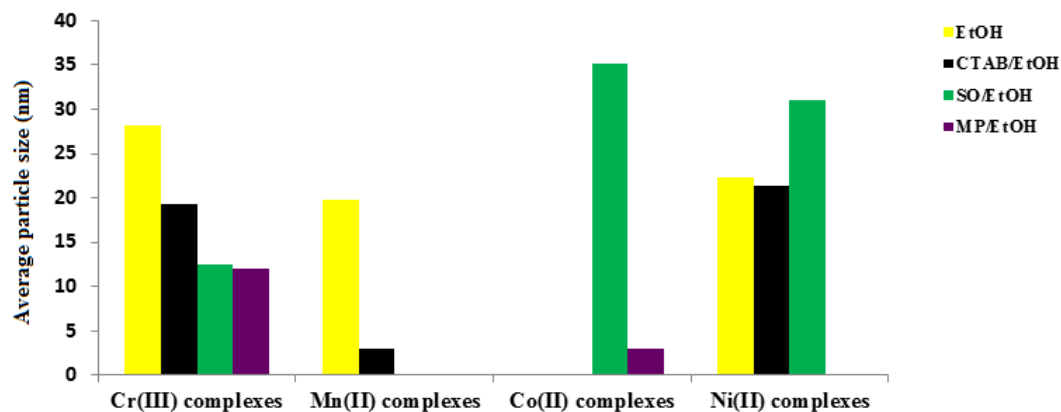


Figure 9: The average particle size of nano-sized Cr(III), Mn(II), Co(II) and Ni(II) complexes using XRD pattern.

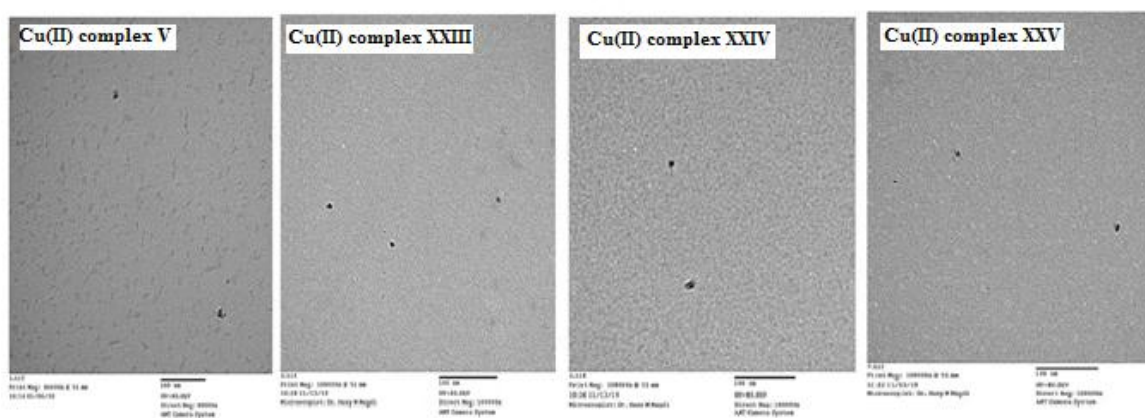


Figure 10: TME images of the nano-sized Cu(II) complexes V, XXIII, XXIV and XXV.

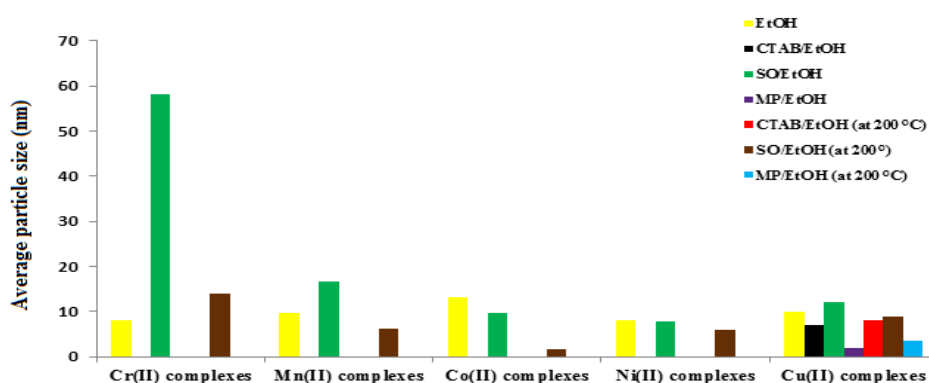


Figure 11: The average particle size of nano-sized Cr(III), Mn(II), Co(II), Ni(II) and Cu(II) complexes using TEM.

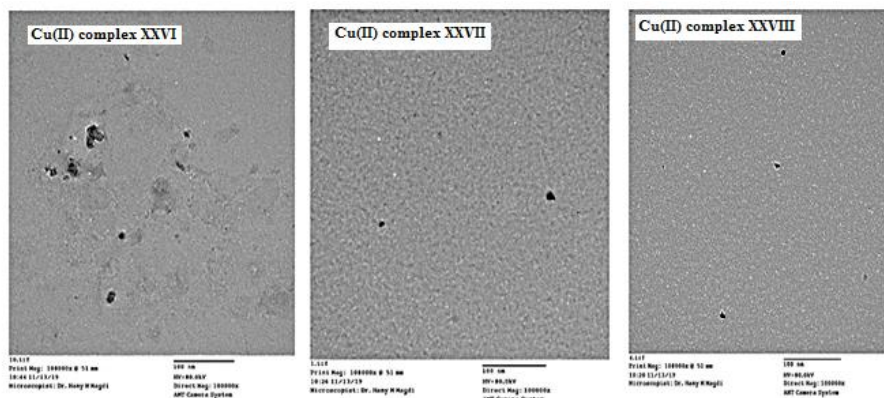


Figure 12: TEM images of the nano-sized Cu(II) complexes XXVI, XXVII and XXVIII.

### 3.2.9. Molecular Modeling and DFT Calculation Studies

Geometrical optimizations of the ligand, H<sub>2</sub>L, and its metal complexes **I**, **II**, **III**, **IV**, **V**, **VI**, Figures 13 - 19, were performed using DMOL3 program in materials studio package which is designed for the realization of density functional theory (DFT) calculation. Also, the bond lengths and bond angles were calculated from the optimized structures. Some selected bond lengths and bond angles were shown in Table 5 and 6. The obtained values revealed that the bond lengths of the ligand were different than that in the complexes, especially for azomethine N-atom, C(2)-N(23), C(24)-N(23) = 1.399, 1.323 Å, and naphtholate O-atom, C(30)-O(31) = 1.350 Å, which coordinated with the metal ions [43]. The calculated azomethine (C=N) and naphtholate (C-O) bond lengths in all metal complexes were found to be in the range 1.320 - 1.500 and 1.296 - 1.395 Å, respectively, indicating slightly elongation of these bonds due to coordination with the metal ions. The lengths of M-N and M-O bonds (that between the metal ions and coordinated azomethine N- and naphtholate O- atoms) were calculated and found to be in the range 1.927 - 2.181 and 1.937 - 2.894 Å, respectively. Also, the bond angles of the ligand were altered upon complexation. A greater change takes place for the angles that involving the coordinated azomethine N- and naphtholate O- atoms, confirming the bonding of them with the metal ions. The evaluated bond angles around the metal ions in the complexes **I**, **III** and **V** (as representative examples) were Cl(74)-Cr(14)-O(72) = 79.025, Cl(74)-Cr(14)-N(50) = 93.327, Cl(74)-Cr(14)-O(48) = 94.134, Cl(74)-Cr(14)-O(13) = 175.299, Cl(74)-Cr(14)-N(12) = 96.564, O(72)-Cr(14)-N(50) = 165.251, O(72)-Cr(14)-O(48) = 84.668, O(72)-Cr(14)-O(13) = 96.332, O(72)-Cr(14)-N(12) = 86.843, N(50)-Cr(14)-O(48), 83.319, N(50)-Cr(14)-O(13) = 91.037, N(50)-Cr(14)-N(12) = 106.696, O(48)-Cr(14)-O(13) = 84.634, O(48)-Cr(14)-N(12) = 164.831, O(13)-Cr(14)-N(12) = 83.834; O(41)-Co(15)-Cl(16) = 106.451, O(41)-Co(15)-O(14) = 114.251, O(41)-Co(15)-N(13) = 96.102, Cl(16)-Co(15)-O(14) = 123.649, Cl(16)-Co(15)-N(13) = 120.131, O(14)-Co(15)-N(13) = 92.954 and O(38)-Cu(14)-Cl(15) = 98.626, O(38)-Cu(14)-O(13) = 87.169, O(38)-Cu(14)-N(12) = 92.817, Cl(15)-Cu(14)-O(13) = 128.334, Cl(15)-Cu(14)-N(12) = 138.005, O(13)-Cu(14)-N(12) = 92.303°, respectively, indicating the octahedral geometry around Cr(III) ion, tetrahedral geometry around Co(II) ion and square planar geometry around Cu(II) ion, which in agreement with the obtained experimental results.

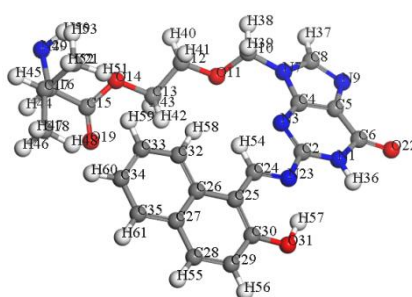
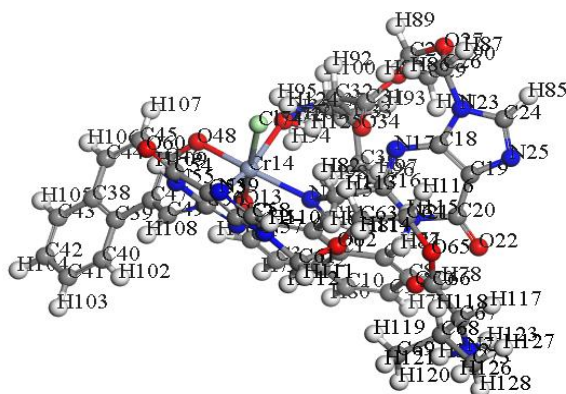


Figure 13: The optimized structure of the ligand, H<sub>2</sub>L.



**Figure 14:** The optimized structure of complex I.

**Table 5:** Some selected calculated bond lengths of the ligand HNABP ( $H_2L$ ) and its metal complexes.

No.	Compound	Bond	Length (Å)	Bond	Length (Å)
	$H_2L$	C(24)-N(23)	1.323		
		C(2)-N(23)	1.399		
		C(30)-O(31)	1.350		
I	[Cr(HNABP) <sub>2</sub> (H <sub>2</sub> O)Cl]3H <sub>2</sub> O	C(11)-N(12)	1.320	N(50)-Cr(14)	2.106
		N(12)-C(15)	1.500	Cl(74)-Cr(14)	2.372
		C(5)-O(13)	1.307	O(13)-Cr(14)	1.954
		C(49)-N(50)	1.337	O(48)-Cr(14)	1.988
		N(50)-C(56)	1.421	O(72)-Cr(14)	2.161
		C(46)-O(48)	1.305		
II	[Mn(HNABP) <sub>2</sub> (H <sub>2</sub> O) <sub>2</sub> ].2H <sub>2</sub> O	N(12)-Cr(14)	2.181		
		C(11)-N(12)	1.332	N(49)-Mn(14)	2.044
		N(12)-C(15)	1.422	O(13)-Mn(14)	2.003
		C(5)-O(13)	1.308	O(47)-Mn(14)	1.937
		C(48)-N(49)	1.340	O(71)-Mn(14)	2.200
		N(49)-C(55)	1.402	O(72)-Mn(14)	2.156
III	[Co(HNABP)(EtOH)Cl]H <sub>2</sub> O	C(45)-O(47)	1.313		
		N(12)-Mn(14)	2.070		
		C(11)-N(13)	1.335		
		C(17)-N(13)	1.403		
		C(5)-O(14)	1.306		
		N(13)-Co(15)	2.014		
IV	[Ni(HNABP) <sub>2</sub> (H <sub>2</sub> O) <sub>2</sub> ]3H <sub>2</sub> O	Cl(16)-Co(15)	2.197		
		O(14)-Co(15)	1.975		
		O(41)-Co(15)	2.157		
		C(11)-N(12)	1.379	N(49)-Ni(14)	1.927
		N(12)-C(15)	1.399	O(13)-Ni(14)	2.894
		C(5)-O(13)	1.384	O(47)-Ni(14)	2.116
V	[Cu(HNABP)(H <sub>2</sub> O)Cl]	C(48)-N(49)	1.340	O(71)-Ni(14)	2.488
		C(55)-N(49)	1.408	O(72)-Ni(14)	2.695
		C(45)-O(47)	1.395		
		N(12)-Ni(14)	1.928		
		C(11)-N(12)	1.325		
		N(12)-C(16)	1.411		
VI	[Zn(HNABP)(H <sub>2</sub> O)Cl].2.5H <sub>2</sub> O	C(5)-O(13)	1.298		
		N(12)-Cu(14)	1.969		
		Cl(15)-Cu(14)	2.115		
		O(13)-Cu(14)	1.955		
		O(38)-Cu(14)	2.481		
		C(11)-N(12)	1.340		
		N(12)-Zn(14)	2.063		
		Cl(15)-Zn(14)	2.182		
		O(13)-Zn(14)	2.016		
		O(38)-Zn(14)	2.242		

**Table 6:** Some selected calculated bond angles of the ligand HNABP (H<sub>2</sub>L) and its metal complexes.

No.	Compound	Angle	Degree (°)	Angle	Degree (°)	Angle	Degree (°)
	H <sub>2</sub> L	C(25)-C(24)-N(23)	122.919	N(23)-C(2)-N(1)	114.396		
		C(24)-N(23)-C(2)	117.526	O(31)-C(30)-C(25)	122.888		
		H(54)-C(24)-N(23)	117.841	O(31)-C(30)-C(29)	116.268		
		N(23)-C(2)-N(3)	122.539				
I	[Cr(HNABP) <sub>2</sub> (H <sub>2</sub> O)Cl].3H <sub>2</sub> O	C(15)-N(12)-Cr(14)	120.463	Cl(74)-Cr(14)-N(50)	93.327	O(72)-Cr(14)-N(12)	86.843
		Cr(14)-N(12)-C(11)	123.705	Cl(74)-Cr(14)-O(48)	94.134	N(50)-Cr(14)-O(48)	83.319
		Cr(14)-O(13)-C(5)	136.708	Cl(74)-Cr(14)-O(13)	175.299	N(50)-Cr(14)-O(13)	91.037
		C(56)-N(50)-Cr(14)	118.166	Cl(74)-Cr(14)-N(12)	96.564	N(50)-Cr(14)-N(12)	106.696
		C(49)-N(50)-Cr(14)	121.309	O(72)-Cr(14)-N(50)	165.251	O(48)-Cr(14)-O(13)	84.634
		C(46)-O(48)-Cr(14)	122.934	O(72)-Cr(14)-O(48)	84.668	O(48)-Cr(14)-N(12)	164.831
		Cl(74)-Cr(14)-O(72)	79.025	O(72)-Cr(14)-O(13)	96.332	O(13)-Cr(14)-N(12)	83.834
II	[Mn(HNABP) <sub>2</sub> (H <sub>2</sub> O) <sub>2</sub> ].2H <sub>2</sub> O	C(15)-N(12)-Mn(14)	124.482	O(72)-Mn(14)-N(49)	90.179	O(71)-Mn(14)-N(12)	91.309
		Mn(14)-N(12)-C(11)	121.345	O(72)-Mn(14)-O(47)	178.364	N(49)-Mn(14)-O(47)	88.195
		Mn(14)-O(13)-C(5)	120.331	O(72)-Mn(14)-O(13)	85.424	N(49)-Mn(14)-O(13)	91.154
		C(55)-N(49)-Mn(14)	116.457	O(72)-Mn(14)-N(12)	87.352	N(49)-Mn(14)-N(12)	177.158
		C(48)-N(49)-Mn(14)	123.786	O(71)-Mn(14)-N(49)	90.254	O(47)-Mn(14)-O(13)	94.791
		C(45)-O(47)-Mn(14)	124.167	O(71)-Mn(14)-O(47)	86.117	O(47)-Mn(14)-N(12)	94.278
		O(72)-Mn(14)-O(71)	93.707	O(71)-Mn(14)-O(13)	178.347	O(13)-Mn(14)-N(12)	87.248
III	[Co(HNABP)(EtOH)Cl]H <sub>2</sub> O	Co(15)-N(13)-C(11)	123.248	Cl(16)-Co(15)-N(13)	120.131		
		C(17)-N(13)-Co(15)	116.586	O(14)-Co(15)-N(13)	92.954		
		Co(15)-O(14)-C(5)	124.878				
		O(41)-Co(15)-Cl(16)	106.451				
		O(41)-Co(15)-O(14)	114.251				
		O(41)-Co(15)-N(13)	96.102				
IV	[Ni(HNABP) <sub>2</sub> (H <sub>2</sub> O) <sub>2</sub> ].3H <sub>2</sub> O	Ni(14)-N(12)-C(11)	121.232	O(72)-Ni(14)-N(49)	97.198	O(71)-Ni(14)-N(12)	100.586
		C(15)-N(12)-Ni(14)	118.864	O(72)-Ni(14)-O(47)	81.089	N(49)-Ni(14)-O(47)	89.805
		Ni(14)-O(13)-C(5)	98.408	O(72)-Ni(14)-O(13)	77.201	N(49)-Ni(14)-O(13)	164.384
		C(48)-N(49)-Ni(14)	125.599	O(72)-Ni(14)-N(12)	87.511	N(49)-Ni(14)-N(12)	126.784
		C(55)-N(49)-Ni(14)	116.842	O(71)-Ni(14)-N(49)	89.281	O(47)-Ni(14)-O(13)	75.001
		C(45)-O(47)-Ni(14)	124.74	O(71)-Ni(14)-O(47)	84.016	O(47)-Ni(14)-N(12)	142.885
		O(72)-Ni(14)-O(71)	163.71	O(71)-Ni(14)-O(13)	92.626	O(13)-Ni(14)-N(12)	68.039
V	[Cu(HNABP)(H <sub>2</sub> O)Cl]	C(16)-N(12)-Cu(14)	117.839	Cl(15)-Cu(14)-N(12)	138.005		
		Cu(14)-N(12)-C(11)	123.772	O(13)-Cu(14)-N(12)	92.303		
		Cu(14)-O(13)-C(5)	127.198				
		O(38)-Cu(14)-Cl(15)	98.626				
		O(38)-Cu(14)-O(13)	87.169				
		O(38)-Cu(14)-N(12)	92.817				
VI	[Zn(HNABP)(H <sub>2</sub> O)Cl].2.5H <sub>2</sub> O	C(16)-N(12)-Zn(14)	120.382	Cl(15)-Zn(14)-N(12)	130.428		
		Zn(14)-N(12)-C(11)	120.117	O(13)-Zn(14)-N(12)	89.842		
		Zn(14)-O(13)-C(5)	124.183				
		O(38)-Zn(14)-Cl(15)	102.312				
		O(38)-Zn(14)-O(13)	85.95				
		O(38)-Zn(14)-N(12)	113.329				
		Cl(15)-Zn(14)-O(13)	127.117				

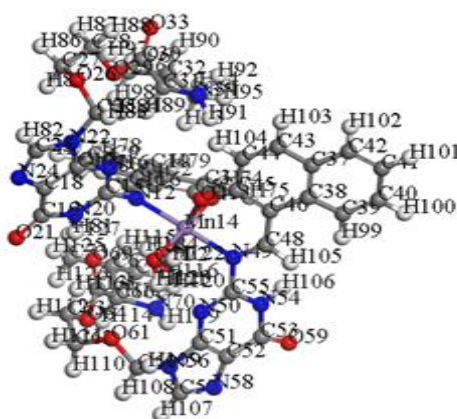


**Figure 15:** The optimized structure of complex II.

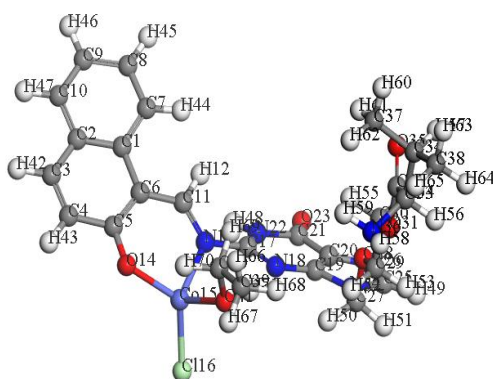


Figure 16: The optimized structure of complex III.

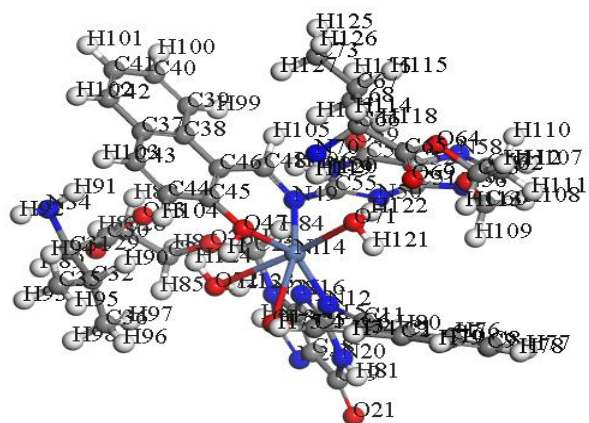


Figure 17: The optimized structure of complex IV.

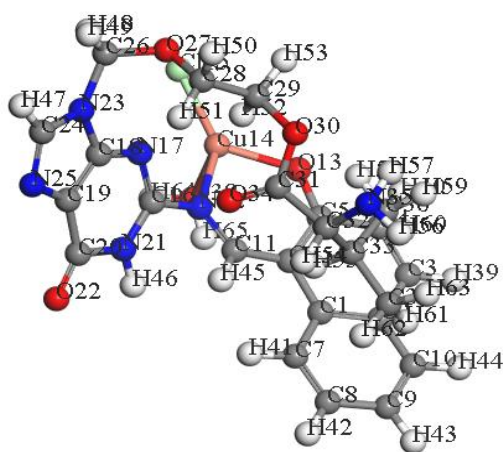
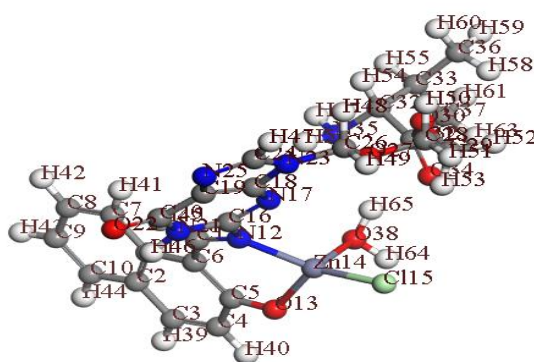


Figure 18: The optimized structure of complex V.



**Figure 19:** The optimized structure of complex VI.

The frontier molecular orbitals, highest occupied molecular orbital (HOMO) and lowest unoccupied molecular orbital (LUMO), are the most important orbitals in a molecule. The frontier orbital energy gap ( $E_{\text{HOMO}} - E_{\text{LUMO}}$ ) is a main parameter to explain the chemical reactivity and chemical stability of the molecule and to determine molecular electrical transport properties [44]. A molecule with a small energy gap ( $\Delta E$ ) is associated with a high chemical reactivity (with a low chemical stability) and also termed as soft molecule [45]. From 3D plots of HOMO and LUMO, Figure 20, the energy gap ( $\Delta E$ ) between the plotted orbitals can be found by using DFT method. The Exact (HOMO – LUMO) gap energies ( $\Delta E$ ) of the ligand and its metal complexes under investigation were evaluated and listed in Table 6. The obtained energy gap ( $\Delta E$ ) values suggesting that the order of chemical reactivity of the ligand,  $\text{H}_2\text{L}$ , in comparison with its metal complexes is: Complex **IV** > Complex **V** > Complex **I** > Complex **VI** > Complex **II** >  $\text{H}_2\text{L}$  > Complex **III**. So, Co(II) complex (**III**) is more stable than the free ligand,  $\text{H}_2\text{L}$ , while the other complexes (**I**, **II**, **IV**, **V** and **VI**) are less stable than the free ligand.

Also, the chemical reactivity values: electronegativity ( $\chi$ ), chemical hardness ( $\eta$ ), chemical potential ( $\mu$ ), electrophilicity ( $\omega$ ), and softness ( $S$ ) of the ligand and its metal complexes were calculated by using HOMO and LUMO energy values [ $\chi = -(E_{\text{LUMO}} + E_{\text{HOMO}}) / 2$ ,  $\mu = -\chi = (E_{\text{LUMO}} + E_{\text{HOMO}}) / 2$ ,  $\eta = (E_{\text{LUMO}} - E_{\text{HOMO}}) / 2$ ,  $S = 1 / 2\eta$ ,  $\omega = \mu^2 / 2\eta$ ,  $\sigma = 1 / \eta$ ] [46], and reported in Table 7. The softness ( $S$ ) and electrophilicity ( $\omega$ ) values of Co(II) complex (**III**) are lower than the that of the ligand, supporting that the stability of this complex is greater than the free ligand, in contrast of the other metal complexes.

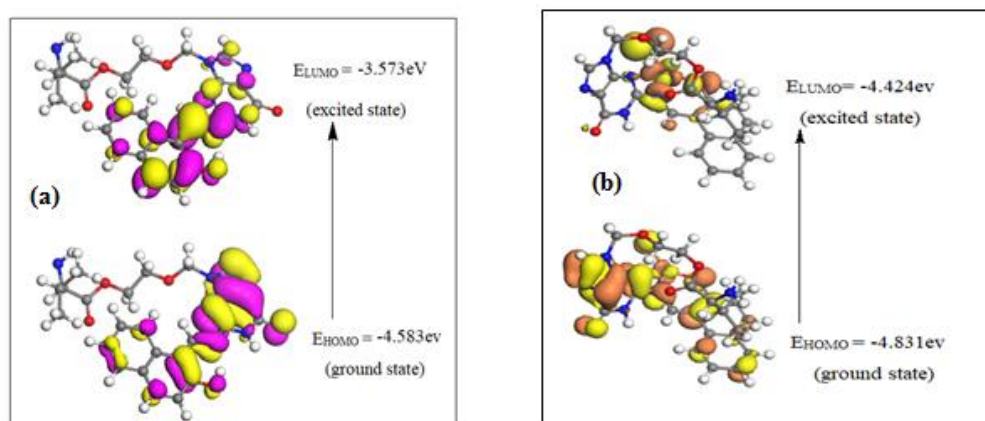


**Figure 20:** 3D plots frontier orbital energies for (a) the ligand,  $\text{H}_2\text{L}$  and its (b) Cu-complex V.

**Table 7:** Evaluated quantum chemical parameters of the ligand HNABP ( $\text{H}_2\text{L}$ ) and its metal complexes.

No.	Compound	HOMO (ev)	LUMO (ev)	$\Delta E$ (ev)	$\chi$	$\mu$	$\eta$	$\sigma$	S	$\omega$
	$\text{H}_2\text{L}$	- 3.573	- 4.583	1.01	-4.078	4.078	0.505	1.980198	0.990	16.46543
I	[Cr(HNABP) <sub>2</sub> (H <sub>2</sub> O)Cl].3H <sub>2</sub> O	-4.093	-3.558	0.535	-3.8255	3.8255	0.2675	3.738317757	1.869	27.35411262
II	[Mn(HNABP) <sub>2</sub> (H <sub>2</sub> O) <sub>2</sub> ].2H <sub>2</sub> O	-3.572	-2.803	0.769	-3.1875	3.1875	0.3845	2.600780234	1.300	13.21216678
III	[Co(HNABP)(EtOH)Cl]H <sub>2</sub> O	-4.783	-3.127	1.656	-3.955	3.955	0.828	1.207729469	0.603	9.445667271

IV	[Ni(HNABP) <sub>2</sub> (H <sub>2</sub> O) <sub>2</sub> ].3H <sub>2</sub> O	-3.516	-3.342	0.174	-3.429	3.429	0.087	11.49425287	5.747	67.57494828
V	[Cu(HNABP)(H <sub>2</sub> O)Cl]	-4.831	-4.424	0.407	-4.6275	4.6275	0.2035	4.914004914	2.457	52.61365172
VI	[Zn(HNABP)(H <sub>2</sub> O)Cl].2.5H <sub>2</sub> O	-4.633	-3.914	0.719	-4.2735	4.2735	0.3595	2.781641168	1.390	25.40028129

#### IV. Biological Activity Studies

##### 4.1. Antitumor Activity Studies

The antitumor activity of the ligand, H<sub>2</sub>L, and its nano-sized metal complexes **I**, **II**, **III**, **IV**, **V** (in EtOH), **VIII**, **XII**, **XVI**, **XX**, **XXIV** (in SO/EtOH), **XXIII**(in CTAB/EtOH) and **XXV** (in MP/EtOH) in addition of the nano-sized complexes **X**, **XIV**, **XVIII**, **XXII**, **XXVII** (in SO/EtOH, after heating at 200 °C), **XXVI** (in CTAB/EtOH, after heating at 200 °C) and **XXVIII** (in MP/EtOH, after heating at 200 °C), was investigated in vitro against Hepatocellular carcinoma cell line (HepG-2 cells) along with standard drug cis-platin (IC<sub>50</sub> = 3.27 µg/ml towards HepG-2 cell line) for comparison purposes. HepG-2 cell line was selected because it is the most common among other various types of Carcinomas. The antitumor activity was specified by IC<sub>50</sub> which refers to the concentration of compound that inhibit the tumor cell growth by 50%. The compounds exhibiting IC<sub>50</sub> value below 5.00 µg/ml, within the range of 5.00-10.00 and 10.00-25.00 µg/ml are considered strong, moderate and weak anticancer agents, respectively [47]. The obtained results revealed that all scanned compounds displayed an inhibition of cell viability and their IC<sub>50</sub> (µg/ml) values showed in Figure 21. The nano-sized Cu(II) complexes **V**, **XXIV** and **XXVI** exhibited strong antitumor activities with IC<sub>50</sub> (µg/ml) values taking the following order: Cu(II) complex **XXIV** (1.93) < Cu(II) complex **V** (3.73) < Cu(II) complex **XXVI** (3.84). The nano-sized Cu(II) complex **XXV** (in MP/EtOH) displayed a moderate antitumor activity (IC<sub>50</sub> = 5.60 µg/ml), whereas the ligand, H<sub>2</sub>L, and its other tested complexes showed weak antitumor activities, with IC<sub>50</sub> values in the range 14.20 – 177.00 µg/ml, against Hepatocellular carcinoma cell line (HepG-2). The highest cytotoxic influence of nano-sized Cu(II) complexes may be due to the high ability of Cu(II) ions to bind DNA than other cations, thus reinforcing DNA oxidation [48]. The nano-sized Cu(II) complex **XXIV** (which synthesized in media SO/EtOH) exhibited IC<sub>50</sub> value (1.93 µg/ml) smaller than the standard drug cis-platin (3.27 µg/ml), Figure 22, indicating the high efficiency of this complex as antitumor agent towards HepG-2 cells.

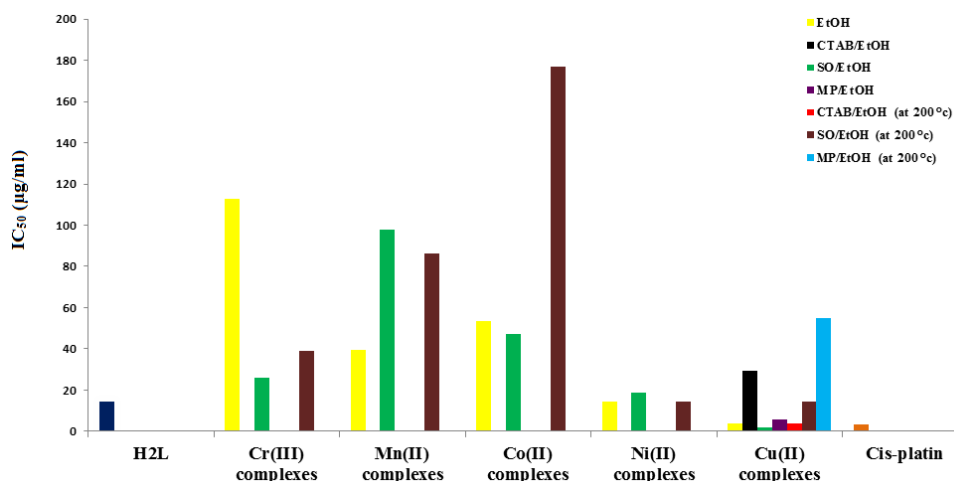


**Figure 21:** In vitro antitumor activity (IC<sub>50</sub>) of the ligand, H<sub>2</sub>L, and its nano-sized Cr(III), Mn(II), Co(II), Ni(II) and Cu(II) complexes against HepG-2.

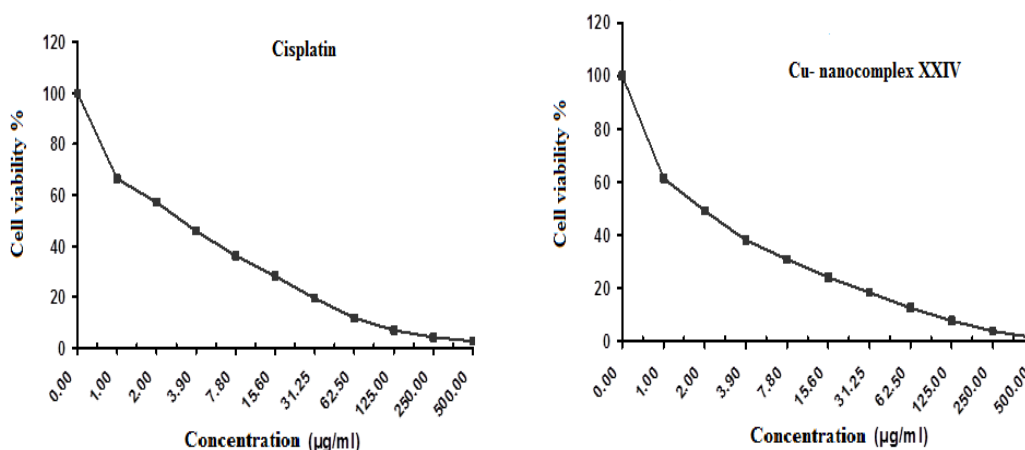


**Figure 22:**The relative cell viability vs. of the cis-platin and nano-sizedCu(II) complex XXIV.

#### 4.2. DNA Cleavage Study

The ability of both nano-sized complexes **V** and **XXIV** to cleavage DNA has been tested by the gel electrophoresis method with two experimental procedures: fixed concentration of DNA with different concentrations of complex, and fixed concentration of complex with different concentrations of DNA. Electrophoretic separation of DNA induced by the complexes **V** and **XXIV** were shown in Figure 23. The obtained results showed the ability of investigated nano-sized complex **V**, at the concentration of 15 µg/ml, to degrade DNA at the concentration of 100 ng, which supporting the activity of this complex as strong antitumor agent capable to DNA-binding, and inhibits growth of the tumor cell. While, the complex **XXIV** has no ability to cleavage DNA at different concentrations. However, the obtained results reveal to another type of binding occurred between the investigated complex **XXIV** and DNA. Where, a non-covalent bond may be formed between the complex and a phosphate group of DNA strands. Formation of this bond led to surrounding of the complex to DNA, in a process called necrosis, which affect on DNA.

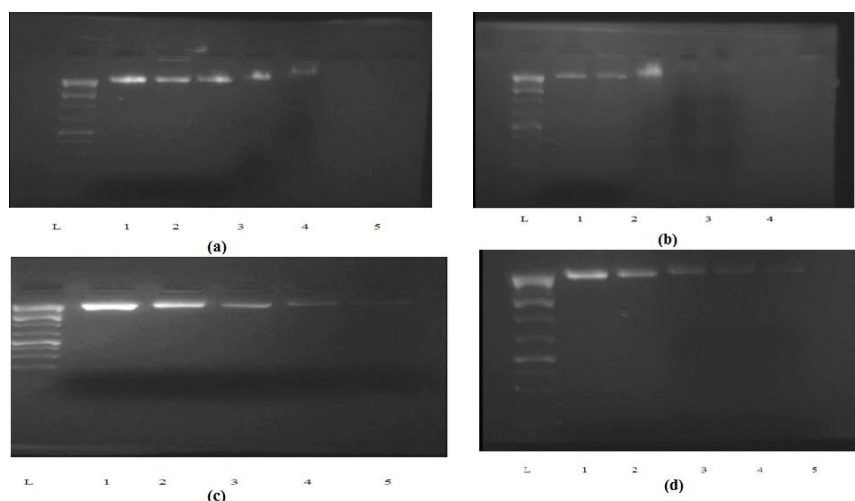


**Figure 23:** Electrophoretic separation of DNA induced by nano-sized Cu(II) complexes **V** and **XXVII**.

(a) Effect of fixed concentration of DNA with different concentrations of complex **V** (Lane L- marker 1kb DNA Ladder, lane 1: DNA control, lane 2: DNA+DMSO, lane 3: 300 ng DNA+5 µg/ml Cu complex **V**, lane 4: 300 ng DNA+10 µg/ml Cu complex **V**, lane 5: 300 ng DNA+15 µg/ml Cu complex **V**), (b) Effect of fixed concentration of complex **V** with different concentrations of DNA (Lane L- marker 1kb DNA Ladder, lane 1: DNA control, lane 2 :DNA+DMSO, lane 3: 300 ng DNA+15 µg/ml Cu complex **V**, lane 4: 200 ng DNA+15 µg/ml Cu complex **V**, lane 5: 100 ng DNA+15 µg/ml Cu complex **V**), (c) Effect of fixed concentration of DNA with different concentrations of complex **XXVII** (Lane L- marker 1kb DNA Ladder, lane 1: DNA control, lane 2: DNA+DMSO, lane 3: 300 ng DNA+5 µg/ml Cu(II) complex **XXVII**, lane 4: 300 ng DNA+10 µg/ml Cu(II) complex **XXVII**, lane 5: 300 ng DNA+15 µg/ml Cu(II) complex **XXVII**), (d) Effect of fixed concentration of complex **XXVII** with different concentrations of DNA (Lane L- marker 1kb DNA Ladder, lane 1: DNA control, lane 2: DNA+DMSO, lane 3: 300 ug DNA+15 µg/ml Cu(II) complex **XXVII**, lane 4: 200 µg DNA+15 µg/ml Cu(II) complex **XXVII**, lane 5: 100 µg DNA+15 µg/ml Cu(II) complex **XXVII**).

### 4.3. Molecular Docking Study

Molecular docking is an effective tool to predict the position and power of interactions between the investigate compounds and DNA [49]. In order to understand the binding modes of the ligand, H<sub>2</sub>L, and its nano-sized Cu(II) complex **V** to DNA, a computational molecular docking study was performed with DNA duplex of the dodecamer sequence (PDB ID: 1BNA) using MOE, 2015.10 software. The obtained data, Table 8, suggesting that the ligand, H<sub>2</sub>L, and its Cu(II) complex **V** interact with DNA helix at the nucleotides: DC-A11, DG-A12, DG-B16, DA-B18 and DC-A9, DG-A10, DA-B17, DT-B19 with binding energy (docking score) of -14.50 and -14.20 kcal/mol, respectively. The interacting groups with DNA were H<sub>2</sub>O, azomethine (C=N), Cl, NH<sub>2</sub> and O-ether, naphtholic-OH, naphthyl-ring, NH<sub>2</sub> for the ligand, H<sub>2</sub>L, and its Cu(II) complex **V**, respectively, by hydrogen bonding, as shown in Figure 24. The docking results revealing strong interactions of both the ligand, H<sub>2</sub>L, and its Cu(II) complex **V** with DNA, which supporting the ability of the nano-sized Cu(II) complex **V** to cleavage DNA and the effective inhibition of this complex toward tumor cells.

**Table 8:** Details for interaction of the ligand, H<sub>2</sub>L, and its nano-sized Cu(II) complex **V** with DNA by molecular docking.

Compound	Docking score S (kcal/mol)	DNA Base	Interacting groups	Type of interaction	H-bond Length (Å)
Ligand, H <sub>2</sub> L	-14.5022	DC-A9	O	H-bond (acceptor)	3.17
		DG-A10	OH	H-bond (donor)	2.97
		DA-B17	Naphthyl	Arene-H	3.69
		DT-B19	NH <sub>2</sub>	H-bond (donor)	3.00
Cu(II) Complex <b>V</b>	-14.2062	DC-A11	OH	H-bond (donor)	2.74
		DG-A12	NH	H-bond (donor)	3.15
		DG-B16	Cl	H-bond (donor)	3.65
		DA-B18	NH <sub>2</sub>	H-bond (donor)	2.99

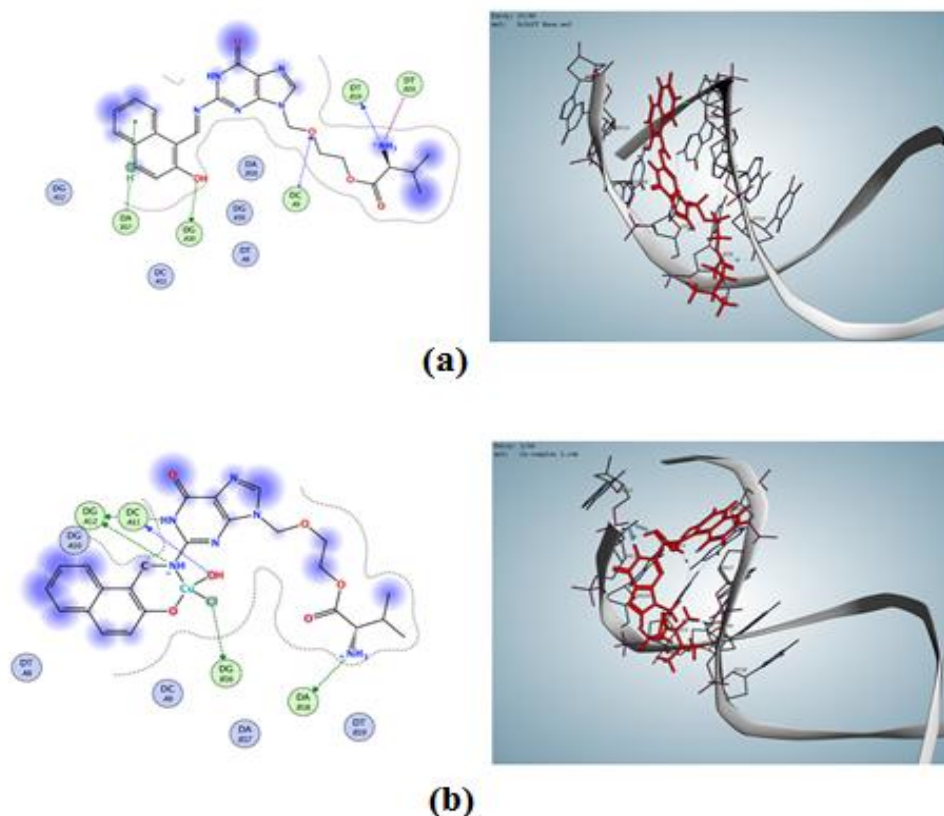


**Figure 24:** 2D & 3D diagrams showing interaction between (a) the ligand, H<sub>2</sub>L, (b) the nano-sized Cu(II) complex **V** and DNA binding site by molecular docking.

### 4.4. Antimicrobial Activity Studies

In vitro antibacterial and antifungal activities of the ligand, H<sub>2</sub>L, and its nano-sized metal complexes **I**, **II**, **III**, **IV**, **V**, **VI** (in EtOH), **VII**, **XI**, **XV**, **XIX**, **XXIII**, **XXIX** (in CTAB/EtOH), **VIII**, **XII**, **XVI**, **XX**, **XXIV**,

**XXX** (in SO/EtOH) and **IX, XIII, XVII, XXI, XXV, XXXI** (in MP/EtOH), were screened against *E. coli* (as a type of Gram negative bacteria), *S. aureus* (as a type of Gram positive bacteria) and *C. albicans* (as a unicellular fungus) along with standard drugs chloramphenicol (inhibition zone = 40 mm), cefoxitin (inhibition zone = 15 mm) and fluconazole (inhibition zone = 30 mm), respectively, for comparison purposes, by applying agar diffusion technique. The obtained results, Figures 25 and 26, indicated that the ligand, H<sub>2</sub>L, is inactive against all tested organisms except towards *E. coli* with inhibition zone 15 mm. Most of investigated metal complexes exhibited good activities against both types of bacteria, *E. coli* and *S. aureus*. The higher activity towards *E. coli* appeared by nano-sized Cu(II) and Co(II) complexes, **V** and **XV**, with equal values of inhibition zone (25 mm), while the higher activity against *S. aureus* appeared by nano-sized Mn(II) and Zn(II) complexes, **XI** and **XXIX**, that exhibited equal values of inhibition zone (27 mm) and higher than the standard drug cefoxitin (15 mm), indicating the high efficiencies of these complexes as antibacterial agents towards *S. aureus*. All metal complexes under investigation did not exhibit antifungal activities towards *C. albicans* except the complexes **VII, IX, XI, XXIV** and **XXIX**, that displayed moderate to high activities with inhibition zone values (mm), 15, 14, 10, 20, 10, respectively, revealed that the nano-sized Cu(II) complex **XXIV** has higher activity towards *C. albicans*. The antimicrobial screening results showed marked enhancement in activity on coordination with the metal ions. Such enhanced activity upon complex formation can be illustrated according to chelation theory [50]. The mode of action of antimicrobial metal complexes with microorganisms may involve interference with the cell wall synthesis, damage as a result of which cell permeability may be altered or they may disorganize the lipoprotein leading to the cell death, or deactivate various cellular enzymes, which play a vital role in different metabolic pathways of these microorganisms. Also, formation of a hydrogen bond through the azomethine group with the active center of the cell constituents, resulting in interference with the normal cell process [51].

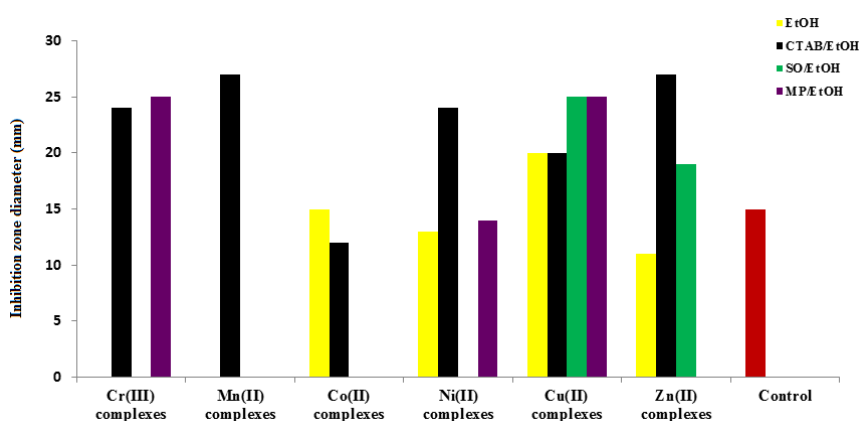


Figure 25: Activities of the nano-sized metal complexes against a Gram positive bacteria (*S. aureus*).

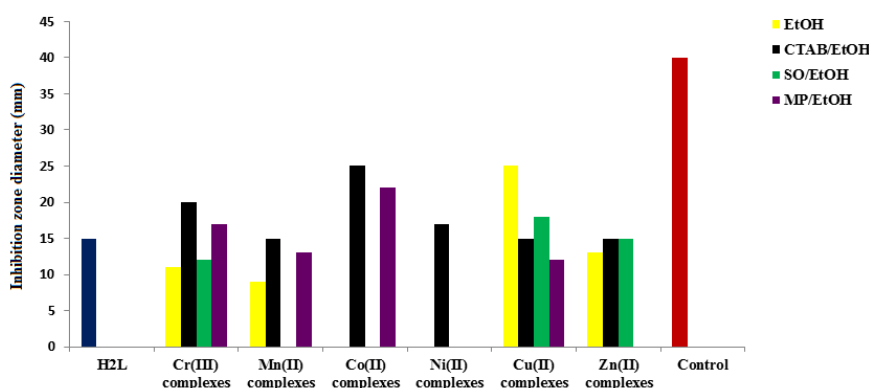


Figure 26: Activities of the ligand, H<sub>2</sub>L, and its nano-sized metal complexes against a Gram negative bacteria (*E. coli*).

### V. Electrical Properties Study

One of the main characteristics of solid compounds is their electrical conductivity [52]. The alternating current conductivity ( $\sigma_{ac}$ ) were measured in the frequency range 0.1 kHz- 8 MHz over the temperature range 308-408 K. The temperature dependence of A.C. conductivity ( $\sigma_{ac}$ ) was described according to Arrhenius relation [53]:  $\sigma = \sigma^0 \exp(-E_a/k_b T)$ , where  $\sigma^0$  is pre exponential conductivity,  $E_a$  is the activation energy of the

conduction process,  $k_b$  is the Boltzmann's constant and  $T$  is the absolute temperature. Variation of A.C. conductivity ( $\sigma_{ac}$ ) of the nano-sized Cu(II) complexes **V**, **XXIII** and **XXVI** at a fixed frequency (10kHz) with temperature were listed in Table 9, and demonstrated in Figure 27. The maximum  $\sigma_{ac}$  values of  $4.05 \times 10^{-2}$ ,  $3.04 \times 10^{-3}$  and  $2.68 \times 10^{-3} \text{ ohm}^{-1}\text{cm}^{-1}$  were recorded at 408, 378 and 408 K, for complexes **V**, **XXIII** and **XXVI**, respectively. These values are about three orders of magnitude for complex **V**, and two orders of magnitude for both complexes **XXIII** and **XXVI**, higher than their room temperature (308 K) values. The plot of  $\ln \sigma_{ac}$  versus  $1/T$  is almost linear in all cases, revealing that the conductivity ( $\sigma_{ac}$ ) of the investigated nano-sized Cu(II) complexes increases with elevating temperature, i.e., these complexes have a positive temperature coefficient of electrical conductivity ( $d\sigma/dT$ ), which indicates that all complexes **V**, **XXIII** and **XXVI** have a semiconducting character within the studied temperature region [54]. The electrical conductivity values (at room temperature, 308 K) taking the following order:

nano-sized Cu(II) complex **V** > nano-sized Cu(II) complex **XXVI** > nano-sized Cu(II) complex **XXIII**.

The activation energies ( $E_a$ ) for the conduction process of the investigated complexes **V**, **XXIII** and **XXVI** were determined from the slopes of Arrhenius plots and summarized in Table 10.

**Table 9:** Variation of A.C. conductivity ( $\sigma_{ac}$ ) of the nano-sized Cu(II) complexes **V**, **XXIII** and **XXVI** (a fixed frequency = 10 kHz) with temperature.

T (k)	A.C. conductivity ( $\sigma_{ac}$ ) $\text{ohm}^{-1}\text{cm}^{-1}$		
	Cu(II) complex <b>V</b>	Cu(II) complex <b>XXIII</b>	Cu(II) complex <b>XXVI</b>
308	$7.93 \times 10^{-5}$	$7.11 \times 10^{-5}$	$7.24 \times 10^{-5}$
318	$1.16 \times 10^{-4}$	$8.22 \times 10^{-5}$	$8.77 \times 10^{-5}$
328	$2.35 \times 10^{-4}$	$1.07 \times 10^{-4}$	$9.38 \times 10^{-5}$
338	$7.14 \times 10^{-4}$	$1.82 \times 10^{-4}$	$1.19 \times 10^{-4}$
348	$2.74 \times 10^{-3}$	$4.96 \times 10^{-4}$	$2.25 \times 10^{-4}$
358	$9.60 \times 10^{-3}$	$1.47 \times 10^{-3}$	$5.74 \times 10^{-4}$
368	$2.06 \times 10^{-2}$	$2.75 \times 10^{-3}$	$1.16 \times 10^{-3}$
378	$2.64 \times 10^{-2}$	$3.04 \times 10^{-3}$	$1.48 \times 10^{-3}$
388	$2.99 \times 10^{-2}$	$2.94 \times 10^{-3}$	$1.87 \times 10^{-3}$
398	$3.53 \times 10^{-2}$	$2.57 \times 10^{-3}$	$2.23 \times 10^{-3}$
408	$4.05 \times 10^{-2}$	$2.43 \times 10^{-3}$	$2.68 \times 10^{-3}$

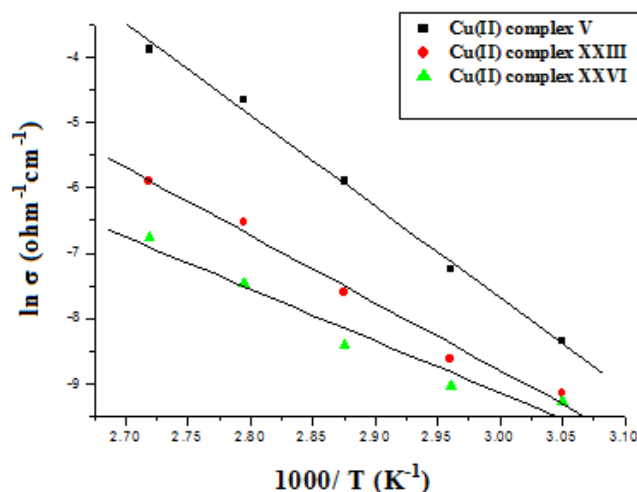


**Figure 27:** Temperature dependence of A.C. conductivity ( $\sigma_{ac}$ ) of the nano-sized Cu(II) complexes **V**, **XXIII** and **XXVI**.

To illustrate the suitable model for conduction mechanism, the charge carrier concentration,  $n$ , and the carrier mobility,  $\mu$ , were calculated using the following relations [55]:  $n = 2(2\pi m^* k_b T/h^2)^{3/2} \exp(-E_a/k_b T)$ ,  $\sigma = ne\mu$ , where  $m^*$  is the effective mass of the charge carrier which is assumed to be equal to the rest mass of an electron,  $k_b$  is Boltzmann's constant,  $E_a$  is activation energy of the conduction process,  $T$  is absolute temperature and  $e$  is the charge of an electron. The expression for  $n$  is valid when the value of  $E_a \geq 3k_b T$ . So  $n$  and  $\mu$  values are only calculated for the samples satisfying these criteria. The charge carrier concentration and carrier mobility of the nano-sized Cu(II) complexes **V**, **XXIII** and **XXVI** were calculated and recorded in Table 10. Variation of charge carrier concentration ( $n$ ) of the investigated complexes **V**, **XXIII** and **XXVI** with temperature was shown in Table 11. An increase in charge carrier concentration with rising temperature was observed in all complexes, which means that the electronic motion as being a thermally activated process in which the electron is displaced to an adjacent localized state. The carrier mobility ( $\mu$ ) value gives an idea about the conduction mechanism in semiconductors. If  $\mu > 1 \text{ cm}^2/\text{Vs}$ , the conduction mechanism is described by band model and if  $\mu < 1 \text{ cm}^2/\text{Vs}$ , the conduction mechanism will be hopping model [55]. The obtained charge carrier mobility values were low enough (less than  $1 \text{ cm}^2/\text{Vs}$ ) to suggest that the conduction occurs by a hopping mechanism. In this model, the electron, or hole, hops from one localized site to next. Whenever it is transferred to another site, the surrounding molecule respond to this perturbation with structural changes and the electron or hole is temporarily trapped in the potential well leading to atomic polarization. The electron resides at this site until it is thermally activated to migrate to another site [56].

**Table 10:** Electronic properties of nano-sized Cu(II) complexes **V**, **XXIII** and **XXVI** at 308 K..

complex	$\sigma_{ac} (\text{ohm}^{-1} \text{cm}^{-1})$	$E_a (\text{ev})$	$n (\text{cm}^{-3})$	$\mu (\text{cm}^2/\text{Vs})$
Cu(II) complex <b>V</b>	$7.93 \times 10^{-5}$	1.203	$1.4 \times 10^{31}$	$3.418 \times 10^{-17}$
Cu(II) complex <b>XXIII</b>	$7.11 \times 10^{-5}$	0.891	$2.10 \times 10^{34}$	$2.11 \times 10^{-20}$
Cu(II) complex <b>XXVI</b>	$7.24 \times 10^{-5}$	0.684	$4.62 \times 10^{37}$	$9.77 \times 10^{-22}$

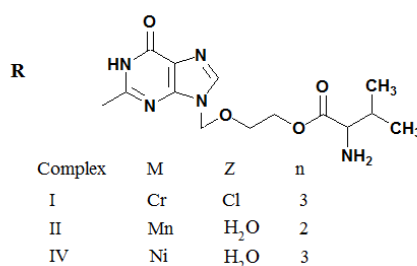
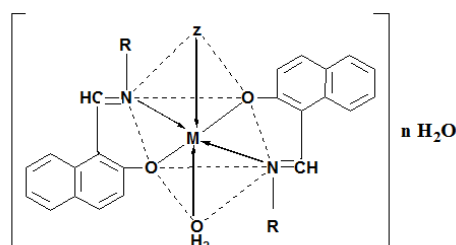
**Table 11:** Variation of charge carrier concentration ( $n$ ) of the nano-sized Cu(II) complexes **V**, **XXIII** and **XXVI** with temperature.

T (k)	charge carrier concentration ( $n$ ) $\text{cm}^{-3}$		
	Cu(II) complex <b>V</b>	Cu(II) complex <b>XXIII</b>	Cu(II) complex <b>XXVI</b>
308	$1.45 \times 10^{31}$	$2.10 \times 10^{34}$	$4.62 \times 10^{37}$
318	$7.66 \times 10^{31}$	$6.32 \times 10^{34}$	$1.09 \times 10^{38}$
328	$30.42 \times 10^{31}$	$1.77 \times 10^{35}$	$2.44 \times 10^{38}$
338	$11.15 \times 10^{32}$	$4.71 \times 10^{35}$	$5.22 \times 10^{38}$
348	$38.00 \times 10^{32}$	$1.18 \times 10^{36}$	$8.44 \times 10^{40}$
358	$12.10 \times 10^{33}$	$2.81 \times 10^{36}$	$17.61 \times 10^{40}$
368	$36.22 \times 10^{33}$	$6.41 \times 10^{36}$	$40.20 \times 10^{40}$
378	$10.23 \times 10^{34}$	$1.40 \times 10^{37}$	$76.45 \times 10^{40}$
388	$27.47 \times 10^{34}$	$2.94 \times 10^{37}$	$129.19 \times 10^{40}$
398	$70.19 \times 10^{34}$	$5.95 \times 10^{37}$	$22.94 \times 10^{41}$
408	$17.15 \times 10^{35}$	$1.16 \times 10^{38}$	$38.81 \times 10^{41}$

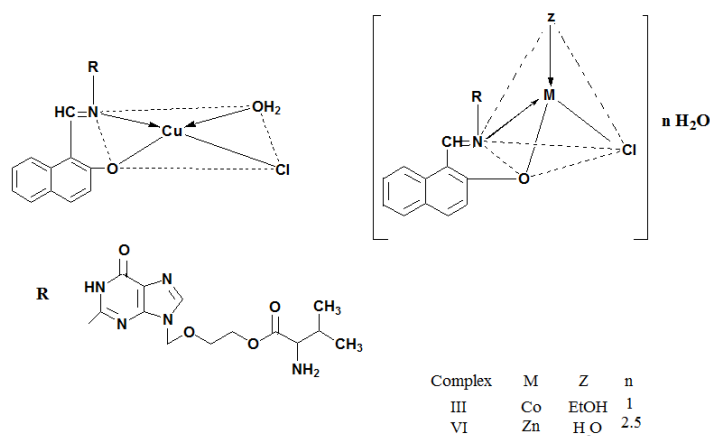
## VI. Conclusion

Nano-sized Cr(III), Mn(II), Co(II), Ni(II), Cu(II) and Zn(II) derived from a new Schiff base ligand,  $\text{H}_2\text{L}$ , were prepared by both chemical and green synthesis. The synthesized complexes were characterized using various analytical and spectral methods. Schiff base ligand,  $\text{H}_2\text{L}$ , behaves as bi-dentate towards the metal ions in a mono-deprotonated form. Octahedral, tetrahedral and square planar arrangements were suggested for the obtained complexes. XRD and TEM results confirmed that the complexes particles are in nano range. The results indicated the bio-efficiency of the investigated complexes as antitumor agents. The nano-sized Cu(II)

complexes act as strong antitumor agents, especially for Cu(II) complex **XXIV**, which exhibited IC<sub>50</sub> value (1.93 µg/ml) smaller than the cis-platin (3.27µg/ml) and has high efficiency as antitumor agent towards HepG-2 cells. Also, the nanosizedCu(II) complex **V** capable to degrade DNA. The docking study supporting strong interaction of the Cu(II) complex **V** with DNA. Most of investigated nano-sized metal complexes exhibited good activities as antimicrobial agents. The electrical conductivity studies indicating that all nano-sized Cu(II) complexes **V**, **XXIII** and **XXVI** have a semiconducting character within the temperature range 308-408 K, and the conduction takes place by a hopping mechanism. The obtained results indicate the suggested structures of the investigated M(II) and M(III) complexes, as shown in Schemes 3 and 4.



**Scheme 3:** Suggested structures of the complexes I, II and IV.



**Scheme 4:** Suggested structures of the complexes III, V and VI.

## References

- [1]. Visor GC, Jackson SE, Kenley RA, Lee GC. Electrochemistry of purine derivatives. 1: Direct determination for the antiviral drug 9-[(1,3-dihydroxy-2-propoxy)methyl]guanine by anodic differential pulse voltammetry. *J. Pharm. Sci.* 1985;74(10):1078-81.
- [2]. Crooks RJ, Murray A. *Antiviral Chemistry and Chemotherapy.* 1994;5(S1):31-37.
- [3]. Kim DK., Lee N, Im GJ, Kim HT, Key HK. *Bioorganic & Medicinal Chemistry.* 1998;6:2525-2530.
- [4]. Ganesh M, Narasimharao CV, Saravana A K, Kamala KK, Vinoba M, Mahajan HS. UV spectrophotometric method for the estimation of valacyclovirHCl in tablet dosage Form. *Journal of Chemistry.* 2009;6(3):814-818.
- [5]. Shinkai I, Ohta Y, *Bioorg. New drugs--reports of new drugs recently approved by the FDA. Alendronate.* *Med. Chem.* 1996;4(1):3-4.
- [6]. Jadhav AS, Pathare DB, Shingare MS. *Journal of pharmaceutical and Biomedical Analysis.* 2007;43(4):1568-1572.
- [7]. Apostolova M, Nachev C, Koleva M, Bontchev PR, Kehaiov I. New competitive enzyme-linked immunosorbent assay for determination of metallothionein in tissue and sera. *Talanta* 1998;46:325-333.
- [8]. Franz KJ, Metzler-Nolte N. Introduction: metals in medicine. *Chem Rev.* 2019;119:727-729.
- [9]. Wang H, Zhou Y, Xu X, Li H, Sun H. Metalloproteomics in conjunction with other omics for uncovering the mechanism of action of metallodrugs: Mechanism-driven new therapy development. *Current Opinion in Chemical Biology.* 2020;55:171-179.
- [10]. Abdel-Monem Y, Abouel-Enein S. Structural, spectral, magnetic and thermal studies of 5-(thiophene-2-ylmethine azo) uracil metal complexes. *Therm. Anal. Calorim.* 2017;130:2257-2275.

- [11]. Ali N, Khan A, Amir S, Khan N, Bilal M. Synthesis of Schiff bases derived from 2-hydroxy-1-naphth- aldehyde and their TIN(II) complexes for antimicrobial and antioxidant activities. *Chem. Soc. Ethiop.* 2017;31(3):445-456.
- [12]. FalahatiM, Attar F, Sharifi M, Saboury AA, Salihi A, Azize FM, Kostova I, Burda C, PrieceI P, Lopez-Sanche JA, Laurent Sk, Hooshmand N, El-SayedIAM, Gold nanomaterials as key suppliers in biological and chemical sensing, catalysisand medicine.BBA - General Subjects. 2020;1864:129435.
- [13]. Aljabali AA, Akkam Y, Al Zoubi MS, Al-Batayneh KM, Al-Trad B, Abo Alrob O, Alkilany AM, Benamara M, Evans DJ. Synthesis of gold nanoparticles using leaf extract of Ziziphuszizyphusand their antimicrobial activity.Nanomaterials. 2018;8(3):174.
- [14]. Vogel AI. Practical organic chemistry including quantitative organic analysis. 3<sup>rd</sup>ed., Longman,London. 1975.
- [15]. Ismail TM, EL Ghamry MA, Abu-El-Wafa SM, Sallam DF. Synthesis, Characterization, 3D Modeling, Biological Activities of Some Metal Complexes of Novel Sulpha DrugSchiff Base Ligand and Its Nano Cu Complex. *Modern Chemistry.* 2015;3(2):18-30.
- [16]. Ismail TM, Soliman H, Abu-El-Wafa SM, Sallam DF. Synthesis, Characterization, 3D Modeling, Nano Structures, Anti-Microbial and-Anti Cancer Activity Studies of Metal (II) Chelates of a Novel Bioactive Schiff Base Ligand Derived from Sulphaquinoxaline. *Journal of Chemical, Biological and Physical Sciences.* 2016;6(3):751-776.
- [17]. Sallam DF, Ismail TM, TawfikAM, Abu-El-Wafa SM. Novel Schiff base ligand N-(6-chloropyrazin-2-yl)-4-{{(E)-(2-hydroxynaphthalen-1- yl)methylidene] amino} benzenesulfonamide (CPHNMABS), its metal(II) chelates and nanocomplexes: Synthesis, structural characterization, DNA, antitumor, docking studies, antimicrobial activity and conductivity studies. *Journal of Applied chemistey.*2020;13:6-24.
- [18]. Okasha RM, AL-Shaikh NE, Aljohani FS, Naqvi A, Ismail EH. Design of novel oligomericmixed ligand complexes: Preparation, biological applications and the first example of their nanosizedscale. *Int. J. Mol. Sci.* 2019;20:743.
- [19]. Zayed MF, Eisa WH, Hezmab AM, Spectroscopic and antibacterial studies of anisotropic gold nanoparticles synthesized using Malvaparviflora. *Journal of Applied Spectroscopy.* 2017;83(6):1000–1004.
- [20]. Chacko A, Newton AMJ. Synthesis and characterization of valacyclovirHClhybrid solid lipid nanoparticles by using natural oils. *Recent Patents on Drug Delivery & Formulation.* 2019;13(1):46-61.
- [21]. Geary WL.The use of conductivity measurements in organic solvents for the characterisation of coordination compounds.*Coord. Chem. Rev.* 1971;7:81-122.
- [22]. El-ghamry MA, Saleh AA, Khalil SME, Mohammed AA, Mono, bi- and trinuclear metal complexes derived from new benzene-1,4-bis(3-pyridin-2-ylurea) ligand. Spectral, magnetic, thermal and 3D molecular modeling studies. *SpectrochimicaActa part A.* 2013;110: 205-2016.
- [23]. Mahmoud MA, Zaitone SA, Ammar AM, Sallam SA. Synthesis, structure and antidiabetic activity of chromium(III) complexes of metformin Schiff-bases. *J. Mol. Struct.* 2016;1108: 60–70.
- [24]. Nakamoto K. Infrared and ramanspectra of inorganic and coordination compounds, 5<sup>th</sup> ed., John Wiley, New York. 1997.
- [25]. Thankamony M, Mohanan K. Synthesis, spectral studies, thermal decomposition kinetics, reactivity and antibacterial activity of some lanthanide(III) nitrate complexes of 2-(N-indole-2-one)amino-3-carboxyethyl-4,5,6,7-tetrahydrobenzo[b]thiophene. *Indian Journal of Chemistry.* 2007;46(2):247-251.
- [26]. Wen HRA , Zuo JL , Scott TA, Zhou H-C , You X-Z. Synthesis, structure andproperties of mercury complexes with a new extended tetraathiafulvalene 4,5-dithiolate ligand. *Polyhedron.* 2005;24:671-677.
- [27]. Raju VP, Vedantham R, Khunt MD, Mathad VT, Dubey PK, Chakravarthy AK. An efficient and large scale process for synthesis of valacyclovir. *Asian journal of chemistry.* 2010;22(5):4092-4098.
- [28]. ZülfiKarog̃lu A, Ataol Y , Çelikoglu E, Çelikoglu U, Idil O. New Cu(II), Co(III) and Ni(II) metal complexes based on ONO donor tridentate hydrazone: Synthesis, structural characterization, and investigation of some biological properties. *J. Mol. Struct.* 2020;1199:127012.
- [29]. Cui M, Chen Y, Xie Q, Yang D, Han M. Synthesis, properties and applications of noble metal iridium nanomaterials. *Coordination Chemistry Reviews.* 2019;387:450–462.
- [30]. El-Sonbati AZ, Diab MA, Morgan ShM, Abou-Dobara MI, El-Ghettany AA. Synthesis, characterization, theoretical and molecular docking studies of mixed-ligand complexes of Cu(II), Ni(II), Co(II), Mn(II), Cr(III), UO2(II) and Cd(II). *J. Mol. Struct.* 2020;1200:127065.
- [31]. Alaghaz AMA, Zayed ME, Alharbi SA, Ammar RAA, Chinnathambi A. Synthesis, spectroscopic identification, thermal, potentiometric and antibacterial activity studies of 4-amino-5-mercapto-S-triazole Schiff's base complexes. *J. Mol. Struct.* 2015;1087:60-67.
- [32]. Ismail TMA, Saleh AA. Synthesis, spectral and magnetic studies of binuclear Mn (II), Co (II), Ni (II) and Cu (II) complexes with hydrazone ligands derived from 1, 4-dihydrazinophthalazine. *Egypt. J. Chem.* 2000;43(3):227-236.
- [33]. Abou El-Enein SA. Polymeric and sandwich Schiff's bases complexes derived from 4,4'-methylenedianiline Characterization and thermal investigation. *J Therm. Anal. Calorim.* 2008;91(3):929-936.
- [34]. Cotton FA, Wilkinson G. Advanced inorganic chemistry, 3<sup>rd</sup> ed., John Wiley, New York. 1972: 541.
- [35]. Esmaielzadeh S, Zarenezhad E. Copper(II) Schiff base complexes with catalyst property: Experimental, theoretical, thermodynamic and biological studies. *ActaChim. Slov.* 2018; 65:416–428.
- [36]. Knittl ET, Abou-Hussein AA. Syntheses, characterization, and biological activity of novel monoand binuclear transition metal complexes with a hydrazone Schiff base derived from a coumarin derivative and oxalyldihydrazine complexes with a hydrazone Schiff base derived from a coumarin derivative and oxalyldihydrazine. *Monatsh Chem.* 2018;149(2):431–443.
- [37]. Jasinski JP, Bianchani JR, Cuva J, El-said FA, El-Asmy AA, West DX. *Anorg. Allg Z, Chem.* 2003;629:202-206.
- [38]. Tudor R, Elena PM, Catalin. Some new Cu(II) complexes containing an ON donor Schiff base: Synthesis, characterization and antibacterial activity. *Polyhedron.* 2011;30:154-162.
- [39]. Hamed MY, Neilands JB. An electron spin resonance study of the Mn(II) and Cu(II) complexes of the Fur repressor protein. *Journal of Inorganic Biochemistry.* 1994;53:235-248.
- [40]. Ghasemi YZ, Takjoo R, Ramezani M, Magee, JT. Molecular design and synthesis of new dithiocarbazate complexes; Crystal structure, bioactivities and nano studies. *RSC Advances.* 2018;8(73):41795-41809.
- [41]. Parsae Z, Mohammadi K. Synthesis, characterization, nano-sized binuclear nickel complexes, DFT calculations and antibacterial evaluation of new macrocyclic Schiff base compounds. *J. Mol. Struct.* 2017;1137:512-523.
- [42]. AlaghazAMA, Aldulmani SAA. Preparation, structural characterization and DNA binding/cleavage affinity of new bioactive nano-sized metal (II/IV) complexes with oxazon-Schiff's base ligand. *Appl. Organometal. Chem.* 2019;33:5135-5154.
- [43]. El-Gammal, AO, Al-Hossainy, FA, El-Brashy AS. Spectroscopic, DFT, optical band gap, powder X-ray diffraction and bleomycin-dependant DNA studies of Co(II), Ni(II) and Cu(II) complexes derived from macrocyclic Schiff base. *J. Mol. Struct.* 2018;1165:177-195.

- [44]. Govindarajan M, Periandy S, Carthigayen K. FT-IR and FT-Raman spectra, thermo dynamical behavior, HOMO and LUMO, UV, NLO properties, computed frequency estimation analysis and electronic structure calculations on  $\alpha$ -bromotoluene. *Spectrochim. Acta Part A*. 2012;97:411-422.
- [45]. Xiao-Hong L, Xiang-Ru L, Xian-Zhou Z. Molecular structure and vibrational spectra of three substituted 4-thioflavones by density functional theory and ab initio Hartree-Fock calculations. *Spectrochim. Acta Part A*. 2011;78:528-536.
- [46]. Ahmed H, Hashim A, Abduljalil HM. Analysis of Optical, Electronic and Spectroscopic Properties of (Biopolymer-SiC) Nanocomposites for Electronics Applications. *Egypt. J. Chem.* 2019;62:1659 – 1672.
- [47]. Shier WT. Mammalian cell culture on \$5 a day: A lab of low cost methods, University of the Philippines, Los Banos .1991.
- [48]. Marzano C, Pellei M, Tisato F, Santini C. Copper complexes as anticancer agents, anti-cancer agents. *Med. Chem.* 2009; 9:185-211.
- [49]. Kavitha B, Sravanthi M, Reddy SP. DNA interaction, docking, molecular modelling and biological studies of o-Vanillin derived Schiff base metal complexes. *Mol. Struct.* 2019;1185:153-167.
- [50]. Thangadurai TD, Natarajan K. Mixed ligand complexes of ruthenium(II) containing  $\alpha$ ,  $\beta$ -unsaturated- $\beta$ -ketoamines and their antibacterial activity. *Trans. Met. Chem.* 2001;26:500-504.
- [51]. Kulkarni A, Avaji PG, Bagihalli GB, Patil SA, Badami PS. Synthesis, spectral, electrochemical and biological studies of Co(II), Ni(II) and Cu(II) complexes with Schiff bases of 8-formyl-7-hydroxy-4-methyl coumarin. *J. Coord. Chem.* 2009;62(3):481-492.
- [52]. Abd El Wahed MG, Metwally SM. Physical studies of some adenine complexes. *Mater. Chem. Phys.* 2003;78:299-303.
- [53]. Sarkar S, Aydogdu Y, Dagdelen F, Bhaumik BB, Dev K. X-ray diffraction studies, thermal, electrical and optical properties of oxovanadium(IV) complexes with quadridentate Schiff bases. *Mater. Chem. Phys.* 2004;88:357-363.
- [54]. Refat MS, El-Deen IM, Zein MA, Adam AA, Kobeas MI. Spectroscopic, structural and electrical conductivity studies of Co(II), Ni(II) and Cu(II) complexes derived from 4-acetylpyridine with thiosemicarbazide. *Int. J. Electrochem. Sci.* 2013;8:9894-9917.
- [55]. Aydogdu Y, Yakuphanoglu F, Aydogdu A, Sekerci M, Alkan C, Aksoy I. XRD, SEM studies and electrical properties of metal complexes, including sodium oxalate ligand ( $\text{Na}_2\text{C}_2\text{O}_4$ ). *Mater. Lett.* 2002;54:352-358.
- [56]. Shriver DF, Atkins PW, Langford C H, "Inorganic Chemistry", Oxford University Press, Oxford, 1996.

Khadija M.Nassir, et. al. " Novel nanoSchiff base M(II) and M(III) complexes derived from antiviral valacyclovir and 2-hydroxy-1-naphthaldehyde (HNAPB). Structural characterization, bio-efficiency, DNA interaction, molecular modeling, docking and conductivity studies." *IOSR Journal of Applied Chemistry (IOSR-JAC)*, 13(5), (2020): pp 01-25.